ISSN 007-2621

No. 2 — 1984

published quarterly

Technical Review

To Advance Techniques in Acoustical, Electrical and Mechanical Measurement

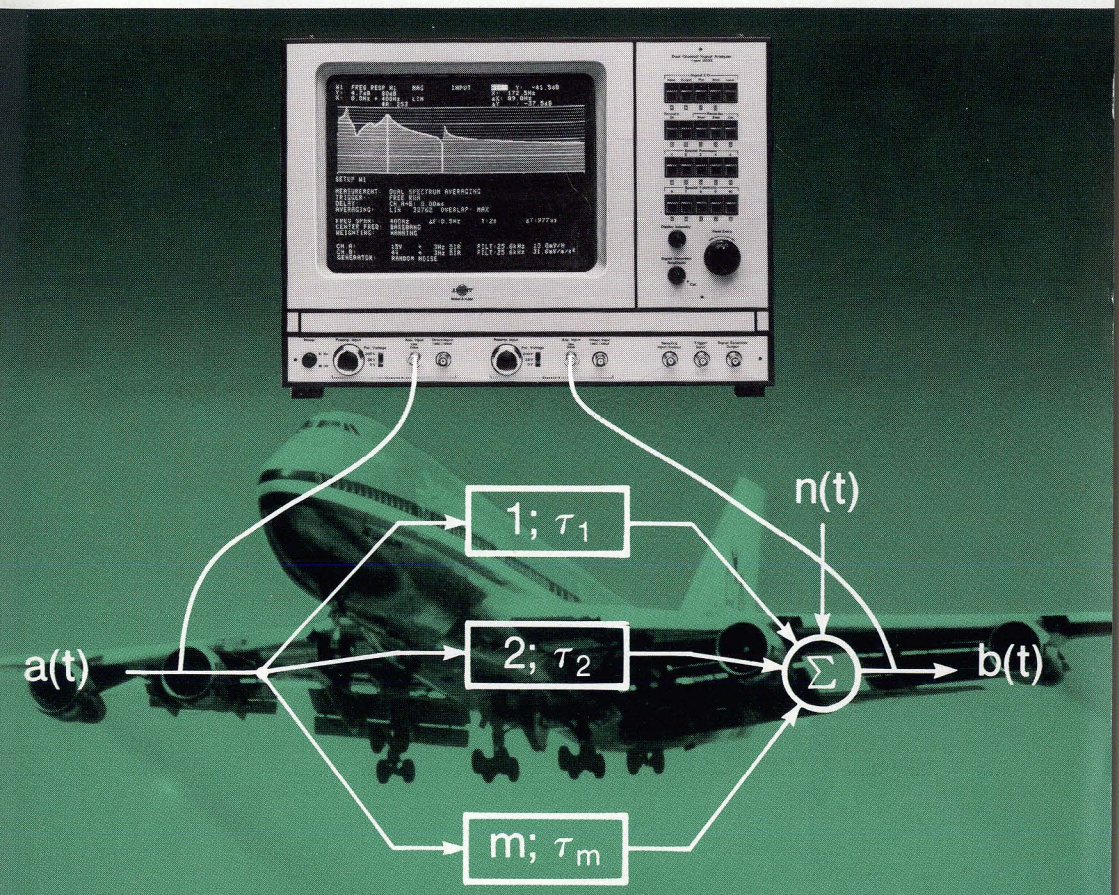

DUAL CHANNEL FFT ANALYSIS (PART II)

Brüel & Kjær

PREVIOUSLY ISSUED NUMBERS OF BRÜEL & KJÆR TECHNICAL REVIEW

1-1984 Dual Channel FFT Analysis (Part I)
4-1983 Sound Level Meters – The Atlantic Divide
Design principles for Integrating Sound Level Meters
3-1983 Fourier Analysis of Surface Roughness
2-1983 System Analysis and Time Delay Spectrometry (Part II)
1-1983 System Analysis and Time Delay Spectrometry (Part I)
4-1982 Sound Intensity (Part II Instrumentation and Applications)
Flutter Compensation of Tape Recorded Signals for Narrow Band Analysis
3-1982 Sound Intensity (Part I Theory).
2-1982 Thermal Comfort.
1-1982 Human Body Vibration Exposure and its Measurement.
4-1981 Low Frequency Calibration of Acoustical Measurement Systems.
Calibration and Standards. Vibration and Shock Measurements.
3-1981 Cepstrum Analysis.
2-1981 Acoustic Emission Source Location in Theory and in Practice.
1-1981 The Fundamentals of Industrial Balancing Machines and their Applications.
4-1980 Selection and Use of Microphones for Engine and Aircraft Noise Measurements.
3-1980 Power Based Measurements of Sound Insulation.
Acoustical Measurement of Auditory Tube Opening.
2-1980 Zoom-FFT.
1-1980 Luminance Contrast Measurement.
4-1979 Prepolarized Condenser Microphones for Measurement Purposes.
Impulse Analysis using a Real-Time Digital Filter Analyzer.
3-1979 The Rationale of Dynamic Balancing by Vibration Measurements.
Interfacing Level Recorder Type 2306 to a Digital Computer.
2-1979 Acoustic Emission.
1-1979 The Discrete Fourier Transform and FFT Analyzers.
4-1978 Reverberation Process at Low Frequencies.
3-1978 The Enigma of Sound Power Measurements at Low Frequencies.
2-1978 The Application of the Narrow Band Spectrum Analyzer Type 2031 to the Analysis of Transient and Cyclic Phenomena.
Measurement of Effective Bandwidth of Filters.
1-1978 Digital Filters and FFT Technique in Real-time Analysis.
4-1977 General Accuracy of Sound Level Meter Measurements.
Low Impedance Microphone Calibrator and its Advantages.

(Continued on cover page 3)

TECHNICAL REVIEW

No. 2 — 1984

Contents

DUAL CHANNEL FFT ANALYSIS (PART II)

by

H. Herlufsen, (M.Sc.)

ƎSTRACT

the first part of this article the basic dual channel FFT measurement was roduced and Frequency Response Function estimates and excitation techques were discussed.

the second part of this article the time domain functions, Impulse Response nction, Autocorrelation and Cross Correlation and their physical interpretation dealt with in some detail. The implementation of the Hilbert Transform on these ne domain functions, to compute the corresponding complex analytical signals, introduced, and the advantages of using the magnitude in the presentation of ese functions in some practical situations are illustrated.

alculation of sound intensity from a dual channel measurement of the sound essure signals from two closely spaced microphones is discussed in terms of vantages and disadvantages.

rmulae for random errors on some of the functions derived from a dual channel easurement on random data are also given.

ƆMMAIRE

a première partie de cet article donnait les notions de base des mesures FFT en -voie, et discutait des estimations des réponses en fréquence et des techniques excitation.

ette deuxième partie traite plus en détail des fonctions du domaine temporel et réponse impulsionnelle, de l'auto-corrélation, de l'intercorrélation et de leur terprétation physique. Elle introduit aussi l'application de la transformée de lbert à ces fonctions temporelles pour calculer les signaux analytiques complexes correspondants, et illustre par quelques cas pratiques les avantages de tilisation de l'amplitude pour la représentation de ces fonctions.

calcul de l'intensité acoustique à partir de la mesure bi-voie de la pression nore de deux microphones rapprochés est traité par comparaison des pours et s contres.

es formules d'erreurs aléatoires sur quelques unes des mesures en bi-voie sur s données aléatoires sont également données.

ZUSAMMENFASSUNG

Der erste Teil dieses Artikels war eine Einführung in die Zwei-Kanal-FFT-Meßtechnik. Es wurden Übertragungsfunktionsnäherungen und Anregungstechniker diskutiert.
Der zweite Teil beschäftigt sich detailierter mit Zeitbereichsfunktionen, Impulsantwort, Autokorrelation und Kreuzkorrelation sowie ihrer physikalischen Interpretation. Die Anwendung der Hilbert-Transformation auf diese Zeitfunktionen zur Berechnung des komplexen analytischen Signals wird vorgestellt und der Vorteil der Darstellung des Betrags dieser Funktionen wird an einigen praktischen Beispielen illustriert.
Die Vor- und Nachteile der Schallintensitätsmessung mit einem Zweikanalsystem und zwei dicht nebeneinander liegenden Druckmikrofonen wird diskutiert.
Zusätzlich werden Formeln für die Berechnung der statistischen Fehler der aus der Messung stochastischer Daten mit dem Zweikanal-System abgeleiteten Funktionen gegeben.

6. Impulse Response Function

The ideal system defined in Section 4 and shown in Fig.14 can be described by its Frequency Response Function $H(f)$ as discussed in Section 4. The corresponding time domain description of the system is given by the Impulse Response Function $h(\tau)$ which can be calculated from the Frequency Response Function by an inverse Fourier Transform.

$$h(\tau) = \mathcal{F}^{-1}\left\{H(f)\right\} = \int_{-\infty}^{\infty} H(f)\, e^{j2\pi f\tau}\, df \qquad (6.1$$

Physically the Impulse Response Function $h(\tau)$ is the response signa from the system caused by an unit impulse input signal at time 0 Mathematically the unit impulse signal is defined by the socalled Dira delta function $\delta(t)$ (see Ref. [3] and [4] for instance).

The Dirac delta function $\delta(t)$ is an impulse at $t = 0$, which is infinitel short in time and infinitely high in amplitude, such that its time integral i unity, i.e.:

$$\int_{-\infty}^{\infty} \delta(t)\, dt = 1$$

The Fourier transform of $\delta(t)$ is unity at all frequencies i.e.

$$\mathcal{F}\left\{\delta(t)\right\} = 1, \quad -\infty < f < \infty$$

which means that all frequencies are excited to the same level if an inpu signal of $a(t) = \delta(t)$ is applied to the system.

According to eq. (1.2) (Part I of this article) we therefore have $B(f) = H(f)$, since $A(f) = 1$ for $a(t) = \delta(t)$. Thus

$$b(t) = \mathcal{F}^{-1}\{H(f)\} = h(t) \text{ for } a(t) = \delta(t) \tag{6.2}$$

Let us now consider a general input signal $a(t)$ to the system and find the output signal $b(t)$ from a time domain description. Any time signal $a(t)$ can be written as a sum of weighted and time shifted delta functions i.e.:

$$a(t) = \int_{-\infty}^{\infty} a(\tau)\,\delta(t-\tau)\,d\tau$$

Each of these weighted and time shifted delta functions $a(\tau)\,\delta(t-\tau)$ at the input will at the output give a signal which is the Impulse Response function, weighted with $a(\tau)$ and shifted τ in time i.e.: $a(\tau)\,h(t-\tau)$. The output signal $b(t)$ from the system, when excited with $a(t)$ at the input, is therefore the superposition of these weighted and time shifted Impulse Response Functions, assuming linearity, giving:

$$b(t) = \int_{\infty}^{\infty} a(\tau)\,h(t-\tau)\,d\tau \;=\; a(t) * h(t) \tag{6.3}$$

$b(t)$ is said to be the convolution of $a(t)$ and $h(t)$. Since $a(t) * h(t) = h(t) * a(t)$, eq.(6.3) is the same as eq. (1.1) (Part I of the article).

It can also be said that eq. (6.3) (or eq.(1.1)) is a direct consequence of the relation: $B(f) = H(f) \cdot A(f)$ (eq.(1.2)) and the Convolution Theorem for the Fourier Transform, which states that multiplication in one domain (here the frequency domain) corresponds to convolution in the other domain (the time domain).

From equation (6.3) we can see that $h(\tau)$ acts as a "memory function" of the system. The output $b(t_o)$ at time t_o not only depends upon the input value at time t_o, $a(t_o)$, but also depends upon the previous values in $a(t)$ weighted with the reversed Impulse Response Function $h(t_o - t)$.

Let us first consider a single degree of freedom system shown in Fig.35, which consists of a mass m supported by a spring, with a spring constant k, and a viscous damper with damping coefficient c. The mass is allowed to move in only one direction x. The input could be the force acting on the mass $f(t)$, while the output could be the displacement $x(t)$. The force caused by the spring is $-kx(t)$ and the damping force is $c\dot{x}(t)$, where $\dot{x}(t)$ is the velocity (time derivative of $x(t)$).

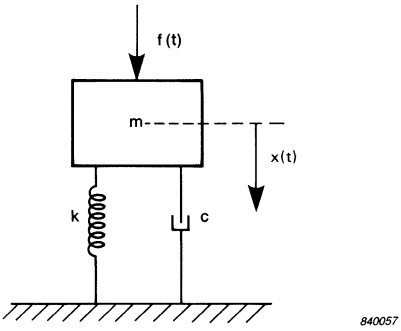

Fig. 35. Mechanical single degree of freedom system

Having the force as the input and the displacement as the output, the Frequency Response Function of the system is the socalled compliance. It is for this simple system given by:

$$H(\omega) = \frac{X(\omega)}{F(\omega)} = \frac{1/m}{-\omega^2 + j\omega\frac{c}{m} + \frac{k}{m}}$$

$$= \frac{A}{j\omega - (j\omega_d - \sigma)} + \frac{A^*}{j\omega - (-j\omega_d - \sigma)} \qquad (6.4$$

where $\omega = 2\pi f$ *and* $X(\omega)$ and $F(\omega)$ are the Fourier Transforms of $x(t)$ and $f(t)$ respectively.

A is a constant and mathematically called the residue for the resonance. It is here imaginary and given by

$$A = \frac{1}{j2m\omega_d} \qquad (6.5$$

In the literature the residue is sometimes defined by $R = j2A$, which is real valued, and (6.4) becomes

$$H(\omega) = \frac{R}{j2\left[j\omega - (j\omega_d - \sigma)\right]} - \frac{R}{j2\left[j\omega - (-j\omega_d - \sigma)\right]} \qquad (6.6$$

The constants ω_d and σ are given by $\omega_d = \sqrt{\frac{k}{m} - \frac{c^2}{4m^2}}$ (6.7

and $\sigma = \frac{c}{2m}$ (6.8

he corresponding Impulse Response Function $h(t)$ is found by an ıverse Fourier Transform of (6.4) or (6.6) and is given by

$$h(t) = 2 \mid A \mid \; e^{-\sigma t} \sin(\omega_d t) \tag{6.9}$$

r

$$h(t) = R \; e^{-\sigma t} \sin(\omega_d t) \tag{6.10}$$

ig.36 shows an example of log $\mid H(f) \mid$ and phase $\phi(f)$ of $H(f)$ and the orresponding $h(t)$ for the single degree of freedom system.

$_d$ is called the damped natural frequency and is the frequency (in ədians per second) of the oscillations in $h(t)$ (see Fig.36). σ is the decay ate determining the exponential decay of $h(t)$, shown as the dotted nvelope curve in Fig.36 (lower graph).

lotice that the higher the damping is in the system the faster is the ecay of the Impulse Response Function $h(t)$ and the shorter will the ffective length of $h(t)$ be.

he socalled undamped natural frequency ω_0 is defined by

$$\omega_0 = \sqrt{\omega_d^2 + \sigma^2} = \sqrt{\frac{k}{m}} \tag{6.11}$$

the system had no damping i.e. $c = 0$, the mass would be oscillating at frequency of ω_0 after an initial impulse excitation.

he damping is also often given by the damping ratio ζ which is defined y

$$\zeta = \frac{\sigma}{\omega_0} \tag{6.12}$$

or $\zeta = 1$ the system is said to be critically damped since in that ituation $\omega_d = 0$ and there will be no oscillations in $h(t)$.

he Impulse Response Function can thus be used for determination of ıe damped natural frequency ω_d, the decay rate σ and the constant A ɔr R) for a single degree of freedom system. A practical example of etermination of decay rate σ will be given later.

ı some acoustical and electroacoustical applications, where an input an be defined and measured, the Impulse Response Function is used

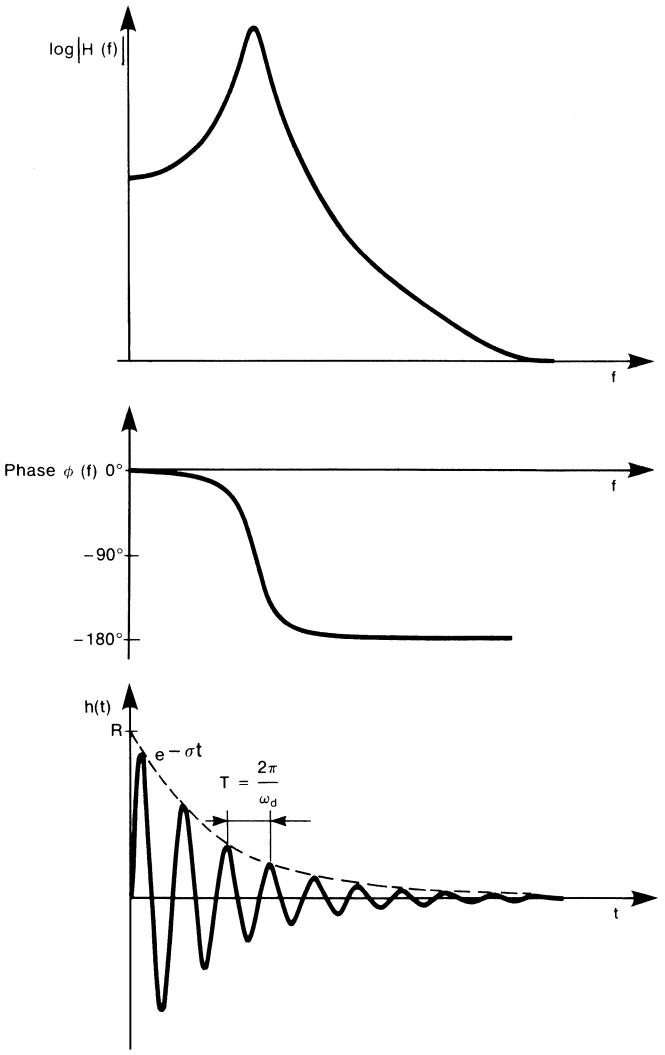

Fig. 36. Logarithmic amplitude log | H(f) | and phase $\phi(f)$ of the Frequency Response Function and corresponding Impulse Response Function of a single degree of freedom system

for determination and recognition of reflections, their time delays and individual magnitudes. For non-dispersive media where no filtering oc-

;urs in the frequency band of interest, reflections will show up as narrow)eaks in the Impulse Response Function at the points in time corre-;ponding to the delay times. The Impulse Response Function can there-ore also be used for identification of transmission paths . This echnique has some advantages compared to the use of Cross Correla-ion Function, which is discussed in Section 7. Since the Impulse Re-;ponse Function describes the system independent of the signals nvolved, the propagation paths can be recognized even though the input ;ignal is shaped in frequency by some filtering. Filtering of the signals vill cause the Cross Correlation Function to be smeared and can herfore make the transmission paths identification difficult. This will be llustrated in Section 7. In order to be able to calculate the Impulse Response Function, however, there has to be some input signal at all the requencies of consideration, since the Frequency Response Function vill be undefined at those frequencies where no input signal exists.

'raditionally the Impulse Response Function hasn't been used very much ;ompared to the Frequency Response Function. $h(t)$ is a real valued unction and is presented on a linear amplitude scale. The dynamic ange of a linear presentation is very limited and oscillations in $h(t)$ due o filtering of the signal in the system often complicates the interpreta-ion of the results.

Vith the implementation of the Hilbert Transform in the time domain, all ne time domain functions including the Impulse Response Function can e made analytical (complex), i.e. they will have a real and an imaginary art. They can therefore be presented in terms of magnitude and phase s well. The Hilbert Transform, which is defined as a convolution ntegral, is used to compute the imaginary part $j\tilde{a}(t)$ of the analytical ignal from the real valued time signal $a(t)$. It is denoted by $\mathscr{H}$ and we ave

$$\tilde{a}(t) = \mathscr{H}\left\{a(t)\right\} = \int_{-\infty}^{\infty} a(\tau)\frac{1}{\pi(t-\tau)}\,d\tau \tag{6.13}$$

nd the socalled analytical time signal $\overset{\nabla}{a}(t)$ is then defined as

$$\overset{\nabla}{a}(t) = a(t) + j\tilde{a}(t) \tag{6.14}$$

he theory behind the Hilbert Transform is defined and discussed in Ref. 2] and [13]. It is found that the Hilbert Transform of a time function can e computed much simpler in the frequency domain compared to a irect calculation in the time domain. The spectrum of the time signal (t) is shifted $-90°$ for positive frequencies and $+90°$ for negative

frequencies. An inverse Fourier Transform of this modified spectrum will result in the time signal $\tilde{a}(t)$, which is the Hilbert Transform of $a(t)$. This technique is used in the B&K Analyzers Type 2032/2034.

Having the complex (analytical) Impulse Response Function

$$\overset{\triangledown}{h}(t) = h(t) + j\tilde{h}(t) \tag{6.15}$$

the magnitude is defined as

$$|\overset{\triangledown}{h}(t)| = \sqrt{h^2(t) + \tilde{h}^2(t)} \tag{6.16}$$

while the phase is given by

$$\theta_h(t) = \text{Arctan}\left(\frac{\tilde{h}(t)}{h(t)}\right) \tag{6.17}$$

The magnitude $|\overset{\triangledown}{h}(t)|$ can be considered as being the envelope of $h(t)$ and this presentation is often much more useful than just the real valued $h(t)$. Firstly, the magnitude does not feature the oscillations often seen in $h(t)$, but gives a smooth curve where identification of reflections, for instance, is much easier and where the peak amplitudes will be correct and consistent. Secondly, the magnitude can be shown on a logarithmic amplitude scale giving more dynamic range in the presentation of the data compared to the conventional linear scale. Fig.37 illustrates this for an acoustical system, where both the input and the output is measured by use of microphones. The Impulse Response Function in this and all the subsequent examples is computed as an inverse Fourier Transform of the Frequency Response Function estimate $H_1(f)$ (see Section 4, Part I of this article). In the upper graph the real valued $h(t)$ is shown, while the lower graph shows the magnitude of the complex $\overset{\triangledown}{h}(t)$ with a logarithmic amplitude scale. The magnitude of $\overset{\triangledown}{h}(t)$ reveals more details in the Impulse Response Function, and the correct levels and time delays for the different reflections are easily found from the magnitude curve.

In this example the input spectrum is band limited but the Impulse Response Function still detects the different reflections as narrow peaks at the different time delays. The Cross Correlation Function for the same signals does not resolve the reflections as clearly as the Impulse Response Function, due to the frequency band limitation. The Cross Correlation Function for the same signals will be shown in Section 7, (Fig.47).

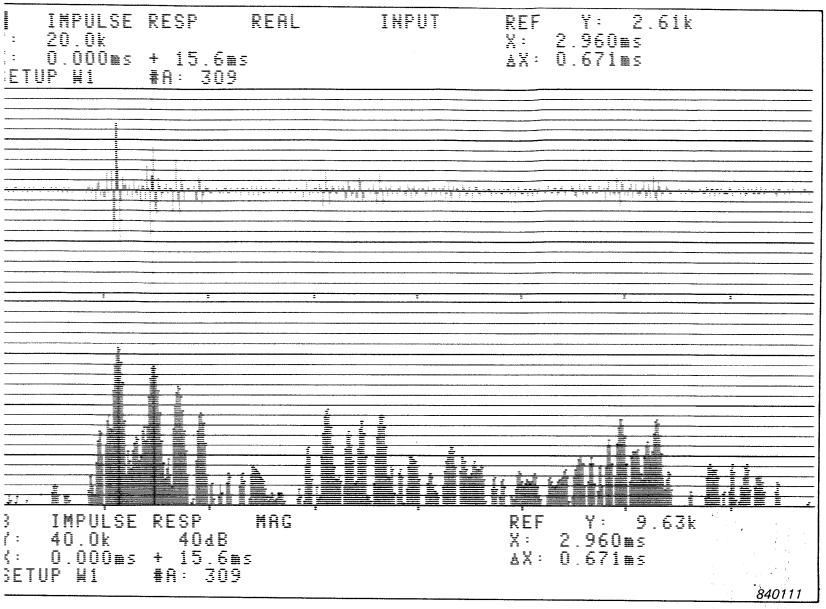

ig. 37. Impulse Response Function of an acoustical system. In the upper graph the real valued h(t) is shown. In the lower graph the magnitude of the complex Impulse Response Function $\tilde{h}(t)$ is plotted on a logarithmic amplitude scale

omputation of the magnitude of the Impulse Response Function was nplemented already several years ago by use of Time Delay Spectrom-try (TDS). The magnitude of $\tilde{h}(t)$ is then often referred to as the Energy ime Curve (ETC). For many acoustical and electroacoustical applica-ons the ETC created new interest and possibilities for the time (delay) omain description of systems (Ref. [13]).

et us return to the application of the Impulse Response Function for etermination of damping, given by the exponential decay in $h(t)$ (6.9) r a single degree of freedom system. When a measurement is per-rmed over a frequency range where the system has several reso-ances, the Impulse Response Function will be complicated and more ifficult to interpret.

ssuming that the system is linear, it can be considered as a combina-on of single degree of freedom systems (Fig.35) and is called a multi

degree of freedom system. The Frequency Response Function is therefore a linear combination of single degree of freedom Frequency Response Functions of the form (6.4), shown in Fig.36. Each resonance is described by the resonance frequency ω_d, the decay rate σ and the constant A (or R) called the residue.

The Impulse Response Function will be the corresponding linear combination of single degree of freedom Impulse Response Functions of the form (6.9), shown in Fig.36 (lower graph), and can therefore be written as

$$h(t) = \sum_r 2\,|A_r|\; e^{-\sigma_r t} \sin\left(\omega_{dr} t\right) \qquad (6.18)$$

or

$$h(t) = \sum_r R_r\; e^{-\sigma_r t} \sin\left(\omega_{dr} t\right) \qquad (6.19$$

where r is the resonance number (mode number).

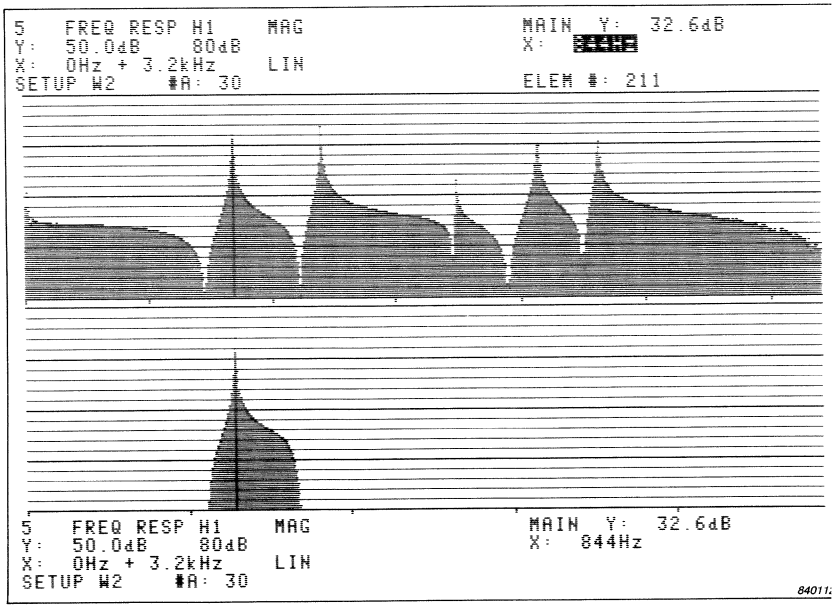

Fig. 38. Frequency Response Function (driving point accelerance of a mechanical system) revealing five resonances (upper graph) Pseudo-random force excitation is used. In the lower graph the first resonance is extracted by use of the weighting function shown in Fig.39.

f the different resonances are well separated in frequency, and the system is lightly damped, each resonance can be treated separately after the measurement, by application of a weighting function on the Frequency Response Function as exemplified in Fig.38. The Frequency Response Function ($H_1(f)$) is here the driving point accelerance for a plate and is measured using shaker excitation. The shaker is attached to the structure via a force transducer and a push rod as shown in Fig.23 Section 5, Part I of the article). A pseudo-random excitation signal is used in order to avoid leakage in the analysis (see Section 4.6). The system is almost linear and the calculated Frequency Response Function in Fig.38 (upper graph) is therefore samples at $f = k \cdot \Delta f = k \cdot 1/T$ of the true Frequency Response Function.

In the lower graph of Fig.38 the first resonance (first mode of vibration) at 844 Hz ($\omega_o \cong \omega_d$ = 5303 rad/s) is extracted by application of a rectangular weighting function, the position and width of which being defined by the user. Some tapering (half-Hanning) is applied in the beginning and at the end of the rectangular weighting in order to avoid sharp edges (truncation) in the edited Frequency Response Function. The weighting function applied in Fig.38 is shown in Fig.39.

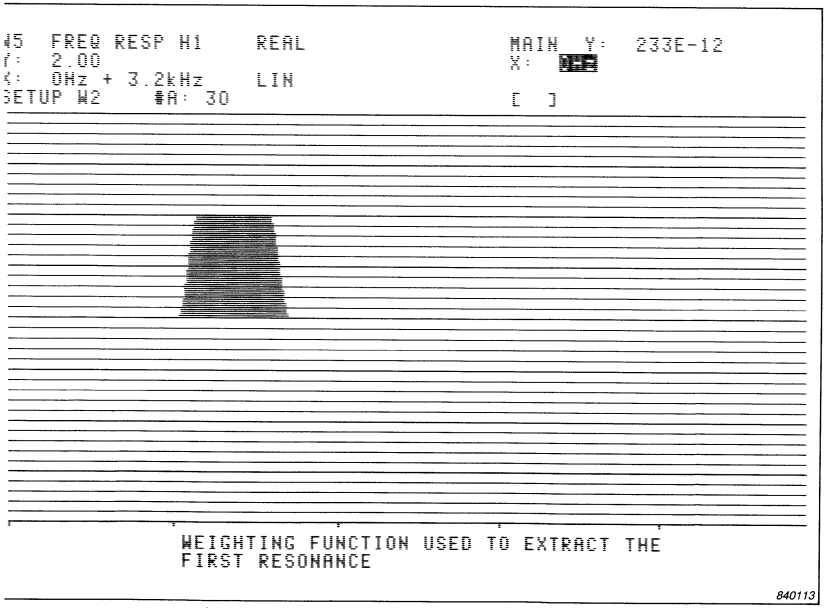

Fig. 39. The user defined weighting function used for extracting the first resonance, as shown in Fig.38.

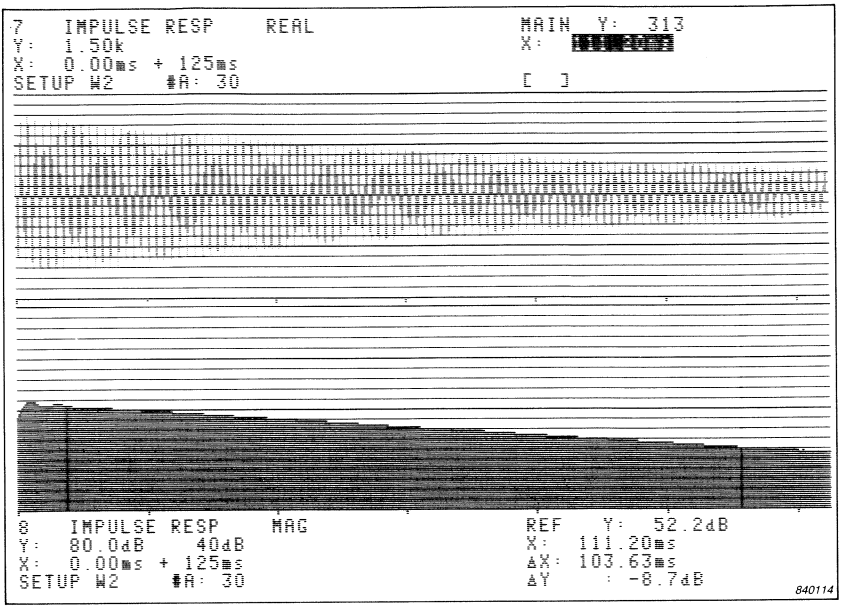

Fig. 40. Real valued Impulse Response Function h(t) (upper graph) and magnitude of complex Impulse Response Function $\hat{h}(t)$, shown on a logarithmic amplitude scale (lower graph), for the first resonance

An inverse Fourier Transform of the edited Frequency Response Function ($H_1(f)$) in the lower graph of Fig.38 results in the Impulse Response Function of this single resonance (first mode of vibration) and is shown in Fig.40 (upper graph). The magnitude of the corresponding complex (analytical) Impulse Response Function, (6.15) and (6.16), is computed and shown in the lower graph of Fig.40, with a logarithmic amplitude scale. The exponential envelope curve $e^{-\sigma t}$, determined by the decay rate σ, can now be seen as a linear decay. The time constant τ of the exponential decay is given by $\tau = 1/\sigma$. The decay corresponding to the time constant τ is given by the factor e^{-1} or in dB: $-20 \log(e) = -8{,}7$ dB.

By use of the reference cursor the time constant τ can be found directly and is for this resonance $\tau_1 = 103{,}6$ ms, as seen from the Δx readout in the lower right corner of Fig.40. The decay rate for this resonance is therefore

$$\sigma_1 = \frac{1}{\tau_1} = 9{,}65\,\text{rad/s}$$

ınd the damping ratio is $\zeta_1 = \frac{\sigma_1}{\omega_{01}} = 0{,}0018.$

ı a similar manner the other resonances can be extracted from the ame measurement and the decay rate of these can be found. In Fig.41, ıe second resonance (second mode of vibration) and the fifth reso- ance (fifth mode of vibration) are extracted using the same kind of veighting function as the one shown in Fig.39 shifted to the relevant esonance.

'he magnitude of the corresponding Impulse Response Functions on ɔgarithmic amplitude scales are shown below the respective edited 'requency Response Functions. The time constants τ_2 and τ_5 are found ɔ be τ_2= 92,0 ms and τ_5 = 48,9 ms (see Δx in the cursor read outs). This ·orresponds to decay rates of
σ_2 = 10,9 rad/s and σ_5 = 20,4 rad/s respectively.

'he undamped natural frequency ω_{0r}, is approximately equal to the lamped natural frequency ω_{dr}, since the damping is light and is 1204 Hz ınd 2312 Hz (i.e. 7565 rad/s and 14527 rad/s) for the two resonances. 'his gives damping ratios of ζ_2 = 0,0014 and ζ_5 = 0,0014 respectively.

'he decay rate for a resonance can also be determined from the half ɔower (3 dB) bandwidth $\Delta f = \frac{\Delta\omega}{2\pi}$ of the resonance peak in the Frequen- :y Response Function, assuming that the resonance is well separated rom other resonances. In this case σ is given by $\sigma = \pi \Delta f$ or in terms of lamping ratio $\zeta = \frac{\pi \Delta f}{\omega_0} = \frac{\Delta f}{2 f_0}$. For lightly damped structures it is nec- ıssary to use a frequency resolution which is high in order to find the ıalf power bandwidth of the resonances. Zoom analysis will therefore ɔften be required and several measurements must be performed in order o cover the frequency range of interest. Using the Impulse Response 'unction calculation in combination with the editing technique as shown, ɔnly one baseband measurement is required in order to find the decay ate (or damping ratio) for the different resonances. Notice however that ɔseudo-random excitation has to be used in order to avoid leakage. .eakage will have the effect of broadening out the resonance peak (see 'ig.10) and the estimated decay rate will therefore be wrong (too high), ıt least when $H_1(f)$ is used for calculation of the Impulse Response 'unction.

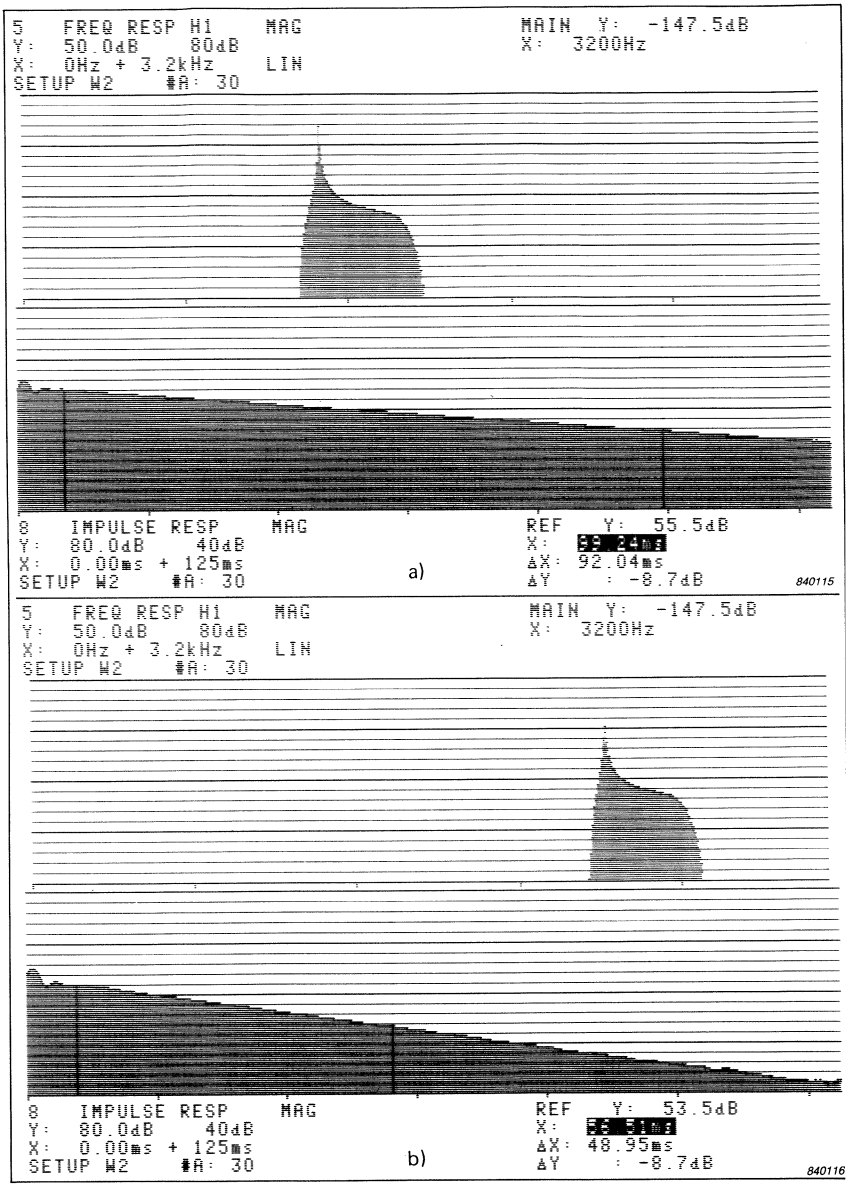

Fig. 41. a) Extraction of the second resonance and the corresponding Impulse Response Function

b) Extraction of the fifth resonance with the corresponding Impulse Response Function.

A zoom analysis, using random noise excitation and a resolution of 0,25 Hz (compared to a resolution of 4 Hz in the baseband measurement) on each of the three resonances (first, second and fifth resonance) gave the following 3 dB bandwidths:

Δf_1 = 3,10 Hz, Δf_2 = 3,15 Hz and Δf_5 = 6,25 Hz

The corresponding decay rates are:
σ_1 = 9,8 rad/s, σ_2 = 9,9 rad/s and σ_5 = 19,7 rad/s,

corresponding quite well with the results from the Impulse Response Functions. Since each zoom analysis is 16 times slower than the baseband analysis (16 times higher resolution) the total analysis time for the three resonances is 3 × 16 = 48 times longer when using zoom analysis compared to the baseband and Impulse Response Function method.

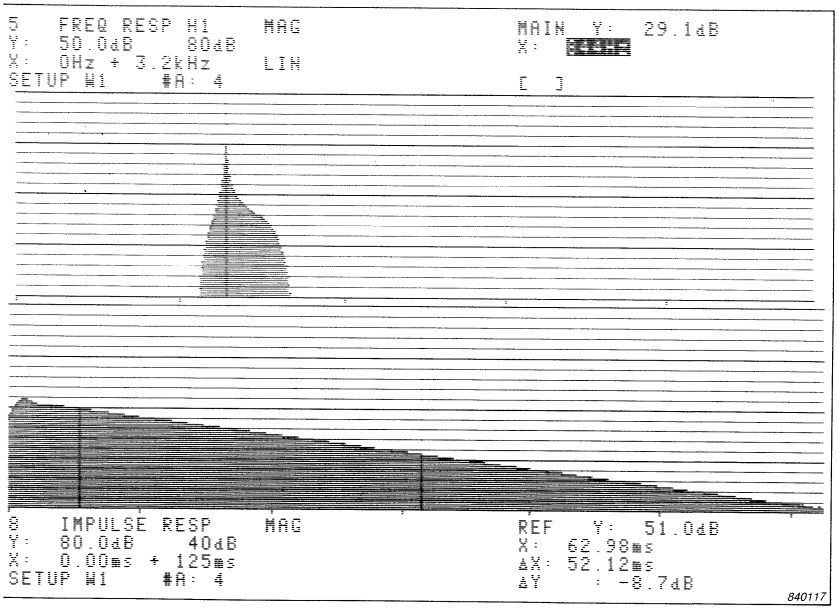

Fig. 42. Same Frequency Response Function as in Fig.38, here measured by use of Impact Hammer excitation. The first resonance is extracted by use of a weighting function (upper graph) and the corresponding Impulse Response Function (magnitude of) is shown with logarithmic amplitude scale in the lower graph

Impact hammer excitation can also be used for the test, and the baseband analysis and Impulse Response Function method can be applied. The extra artificial damping caused by the exponential weighting function, which might be applied on the response signal in Channel B, is known and can be corrected for as explained in Section 5.6. Fig.42 shows the edited driving point accelerance for the same structure, point and direction as used before (Fig.38). The analysis bandwidth of 4 Hz is also the same. The first resonance is extracted by use of the same weighting function as used in the lower graph of Fig.38 and shown in Fig.39. The time constant of the Impulse Response Function is found to be τ_1 = 52,12 ms. The exponential weighting which was applied on the response signal had a length (time constant) of τ_w = 99,97 ms. Thus the true decay rate is

$$\sigma_1 = \frac{1}{\tau_1} - \frac{1}{\tau_w} = 19{,}18\,\text{rad/s} - 10{,}00\,\text{rad/s} = 9{,}18\,\text{rad/s},$$

which is the same, within 5% accuracy, as the decay rate found in the test using pseudo-random excitation with a shaker.

7. Autocorrelation and Cross Correlation

The mathematical definitions of the Autocorrelation Function $R_{aa}(\tau)$ of a signal $a(t)$ and the Cross Correlation Function $R_{ab}(\tau)$ between two signals $a(t)$ and $b(t)$ are given by

$$R_{aa}(\tau) = \lim_{T\to\infty} \frac{1}{T} \int_T a(t)\, a(t+\tau)\, dt \qquad (7.1)$$

$$R_{ab}(\tau) = \lim_{T\to\infty} \frac{1}{T} \int_T a(t)\, b(t+\tau)\, dt \qquad (7.2)$$

Comparing these definitions to the definition of covariance σ_{ab} between two variables a and b given by (3.2) it is seen, apart from the subtraction of the mean values μ_a and μ_b in σ_{ab}, that the Autocorrelation $R_{aa}(\tau)$ is the covariance of the time signal $a(t)$ and a replica of this signal displaced τ in time i.e. $a(t+\tau)$. Likewise, the Cross Correlation $R_{ab}(\tau)$ is the covariance of $a(t)$ and the time signal $b(t)$ with a displacement of τ in time i.e. $b(t+\tau)$.

The practical interpretation of Autocorrelation Function $R_{aa}(\tau)$ is therefore to what degree the time signal $a(t)$ is similar with a displaced version of itself as a function of the displacement τ. Likewise the Cross Correlation Function $R_{ab}(\tau)$ gives a measure of the degree of similarity

between the time signal $a(t)$ and a displaced version of the time signal $b(t)$ as a function of the time displacement τ.

In practice it is often more convenient to work with the normalised Correlation Functions given by:

$$\rho_{aa}(\tau) = \frac{R_{aa}(\tau)}{R_{aa}(0)} \tag{7.3}$$

and

$$\rho_{ab}(\tau) = \frac{R_{ab}(\tau)}{\sqrt{R_{aa}(0)\ R_{bb}(0)}} \tag{7.4}$$

$\rho_{aa}(\tau)$ and $\rho_{ab}(\tau)$ are called the Autocorrelation Coefficient Function and the Cross Correlation Coefficient Function respectively. $R_{aa}(0)$ is the total power in the signal $a(t)$ given by

$$\lim_{T \to \infty} \frac{1}{T} \int_T a^2(t)\, dt$$

and $R_{bb}(0)$ is the total power in the signal $b(t)$ given by

$$\lim_{T \to \infty} \frac{1}{T} \int_T b^2(t)\, dt.$$

It can be shown that $|\rho_{aa}(\tau)| \leqslant 1$ and that $|\rho_{ab}(\tau)| \leqslant 1$ for all τ.

$\rho_{aa}(\tau)$ and $\rho_{ab}(\tau)$ correspond to the Correlation Coefficient ρ_{xy} defined by (3.1).

From (7.1) and (7.2) it is easily shown (using the convolution theorem for the Fourier Transform) that the Autocorrelation Function $R_{aa}(\tau)$ and the Cross Correlation Function $R_{ab}(\tau)$ are related to the Autospectrum $S_{AA}(f)$ and the Cross Spectrum $S_{AB}(f)$ via the Fourier Transform as:

$$R_{aa}(\tau) = \mathcal{F}^{-1}\left\{S_{AA}(f)\right\} = \int_{-\infty}^{\infty} S_{AA}(f)\, e^{j2\pi f\tau}\, df \tag{7.5}$$

and

$$R_{ab}(\tau) = \mathcal{F}^{-1}\left\{S_{AB}(f)\right\} = \int_{-\infty}^{\infty} S_{AB}(f)\, e^{2\pi f\tau}\, df \tag{7.6}$$

When $R_{aa}(\tau)$ and $R_{ab}(\tau)$ are calculated from a dual channel FFT measurement, (7.5) and (7.6) are used as seen in Fig.2 (Section 2). The inverse Fourier Transform performed in practice is of course the inverse DFT (or rather inverse FFT) as discussed in Section 2.1.

Since $S_{AA}(f)$ is real and even $R_{aa}(\tau)$ is also real and even i.e. $R_{aa}(\tau) = R_{aa}(-\tau)$. $R_{ab}(\tau)$ is also real, because $S_{AB}(f)$ is conjugate even, but is in general **not** even, because $S_{AB}(f)$ in general have an imaginary part different from zero.

The obvious applications of the **Autocorrelation Function** are:

a) **Detection of echoes (reflections) in the signal.**
If an echo (reflection) with a time delay of τ_o exists in the signal, the Autocorrelation Function will peak at $\tau = \tau_o$ (apart from at $\tau = 0$) and the value of the Autocorrelation Coefficient Function at τ_o, $\rho_{aa}(\tau_o)$, will give a measure of the relative strength of the echo (reflection). It is here assumed that the signal is a broadband signal, which will become clear shortly.

b) **Detection of periodic signals buried in random noise**
The Autocorrelation Function of a periodic signal is also periodic, since a periodic signal will correlate with itself at a delay of one period T, two periods $2T$, etc. The random background noise signal will have an Autocorrelation Function which diminishes to zero with increasing delay and the periodic signal can therefore be detected after a certain delay time in the Autocorrelation Function.

Fig.43 shows the Autocorrelation Coefficient Function ρ_{aa} for a) broadband random noise, b) sinewave and c) sinewave buried in broadband random noise.

The Autocorrelation Coefficient Function for the broadband random noise diminishes very quickly to zero (Fig.43.a)). This is a consequence of the socalled uncertainty principle for functions related by the Fourier Transform. If the bandwidth of the Autospectrum $G_{AA}(f)$ is Δf and the width of the Autocorrelation Function $R_{aa}(\tau)$ is Δt, the uncertainty principle states that

$$\Delta f \cdot \Delta t \geqslant 1 \qquad (7.7)$$

In the example, Fig.43 a), the bandwidth of the random noise is $\Delta f \approx$ 1040 Hz and it is seen that $\rho_{xy}(\tau) \approx 0$ for $\tau = \Delta t = 1{,}4$ ms $\geqslant \frac{1}{\Delta f} = 0{,}96$ ms.

The Autocorrelation Coefficient Function for the sinewave is a cosine with the same period length T as shown in Fig.43.b). The sinewave correlates 100% with itself with delays of $\tau = 0$, $\tau = 1$ period length, $\tau = 2$ period lengths etc. In Fig.43.b) the period length is 1,251 ms (see cursor readout ΔX).

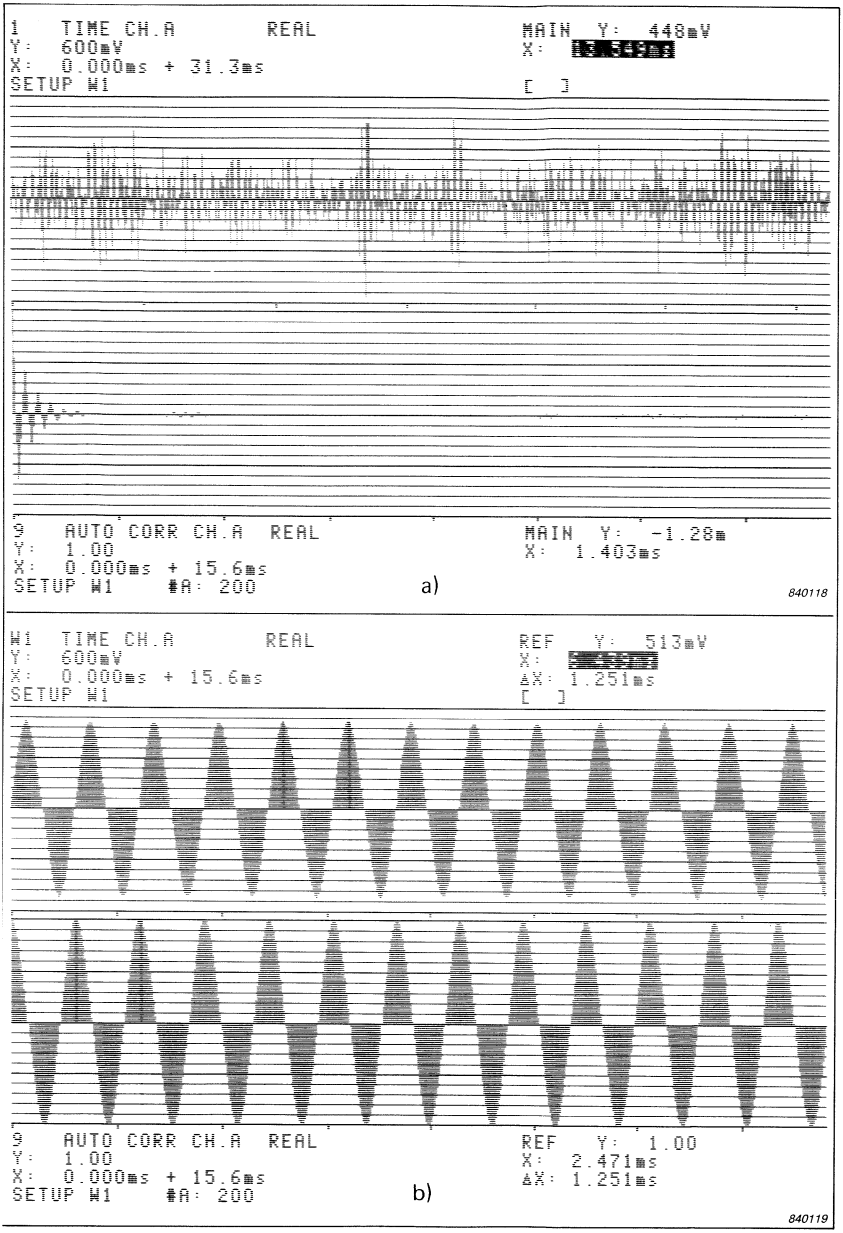

Fig. 43. Autocorrelation Coefficient Function for different types of signals
a) Broadband random noise b) Sine wave

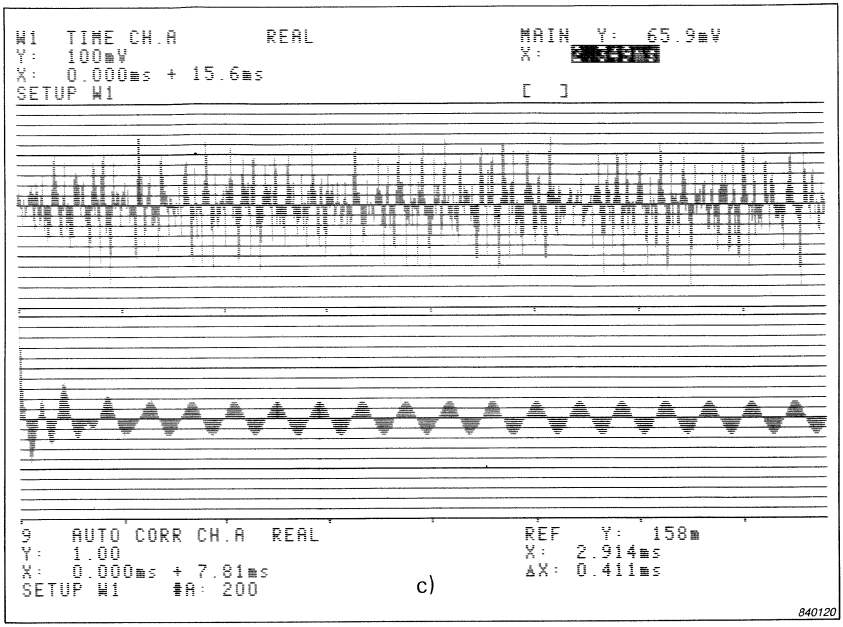

Fig. 43. Autocorrelation Coefficient Function for different types of signals
c) Sine wave buried in broadband random noise

It is thus obvious that detection of echoes (reflections) can only be performed using the Autocorrelation Function if the signal is broadband and with enough bandwidth that the corresponding peaks in the Autocorrelation Function become sufficiently narrow and well separated.

It should be mentioned that for this application, use of the Cepstrum is often preferred over use of the Autocorrelation Function, since the Cepstrum is less sensitive to the shape of the Autospectrum. A description of Cepstrum techniques is found in Ref. [14].

In Fig.43.c) it is seen that the Autocorrelation Coefficient Function detects the periodic signal (a sinewave) which is buried in the random background noise.

If the periodic signal is a signal containing several frequency components it might be more suitable to use the Autospectrum rather than the Autocorrelation Function since the frequencies of the different compo-

nents and their levels are directly detected in the Autospectrum. Zoom analysis might however be required if their levels are very low compared to the background noise level.

The most common applications of **Cross Correlation Function** are the following:

a) **Determination of time delays.** If a signal is propagating from one point A to another point B the Cross Correlation Function $R_{ab}(\tau)$ between the signals $a(t)$ and $b(t)$ at the two points will have a peak at the time displacement corresponding to the time delay (propagation time) τ between the two points. It is assumed that the signals involved are broadband and that the propagation is non-dispersive which means that propagation velocity is independent of frequency. If the velocity depends upon the frequency the propagation is said to be dispersive and this will complicate the situation. There are two possibilities of getting around this problem.

One possibility is to apply a weighting function on the Cross Spectrum (similar to the weighting functions applied on the Frequency Response Function described in Section 6), before the inverse Fourier Transform, in order to find the Cross Correlation Function for only a limited frequency range, where the propagation velocity can be considered as nearly constant. The peak in the Cross Correlation Function will of course be smeared out as a consequence of the uncertainty principle (7.7).

Another possibility is to use the phase of the Cross Spectrum directly, since this is related to the delay time. For a single delay of $\tau_o(f)$ the phase of the Cross Spectrum is $\phi_{AB}(f) = 2\pi f \tau_o(f)$ and the time delay can thus be found as a function of frequency $\tau_o(f)$.

b) **Identification of transmission paths.** If there are several transmission paths for the signal from point A to point B there will be several peaks in the Cross Correlation Function, one peak for each transmission path at a delay time τ_n corresponding to the propagation time τ_n for the n^{th} path. The amplitude of each peak in the Cross Correlation Coefficient Function will give a measure of the relative strength of each transmission path. Again it is here assumed that the signals are broadband and that the propagation is non-dispersive. If the propagation is dispersive, application of weighting functions on

the Cross Spectrum before the inverse Fourier Transform as described under a) might still make identification of transmission paths possible.

c) **Detection of signals buried in extraneous noise.** If a signal $s(t)$, which can be either deterministic or random, is buried in extraneous noise in both $a(t)$ and $b(t)$ i.e. $a(t) = s(t) + n(t)$ and $b(t) = s(t) + m(t)$, where $n(t)$ and $m(t)$ are assumed to be uncorrelated, the Cross Correlation Function $R_{ab}(\tau)$ will only contain information about the correlated part $s(t)$ in $a(t)$ and $b(t)$.

This is because the uncorrelated noise terms $n(t)$ and $m(t)$ at each frequency will be averaged out in the Cross Spectrum $S_{AB}(f)$, which therefore will only contain contribution from the correlated parts in $a(t)$ and $b(t)$ as explained in Section 2.1. In the situation considered here the Cross Correlation Function $R_{ab}(\tau)$ will give the Autocorrelation Function $R_{SS}(\tau)$ of the signal $s(t)$ without any influence from $n(t)$ and $m(t)$.

Fig.44 illustrates the applications a) and b). In this acoustical experiment the input is measured with a microphone close to a sound source and the output is measured with a microphone at a distance of approximately 1,1 m.

The source generates broadband random noise and the input Autospectrum $G_{AA}(f)$ (upper graph of Fig.44) is seen to be fairly flat over the frequency range considered (0–12,8 kHz). The Cross Correlation Coefficient Function $\rho_{ab}(\tau)$, shown in the middle graph, reveals a number of propagation paths (direct sound and reflections). The peaks corresponding to the different paths are narrow, because the signals are broadband and it is quite easy to separate the paths and find their propagation times.

Fig.45 shows similar results when the source is fed by band-limited random noise. The Cross Correlation Coefficient Function $\rho_{ab}(\tau)$ (the graph in the middle) again reveals the different propagation paths, but the peaks are now very broad due to the frequency band limitation of the signals involved. The broadening of the peaks complicates the identification of the different reflections which illustrates one of the difficulties often encountered in practice.

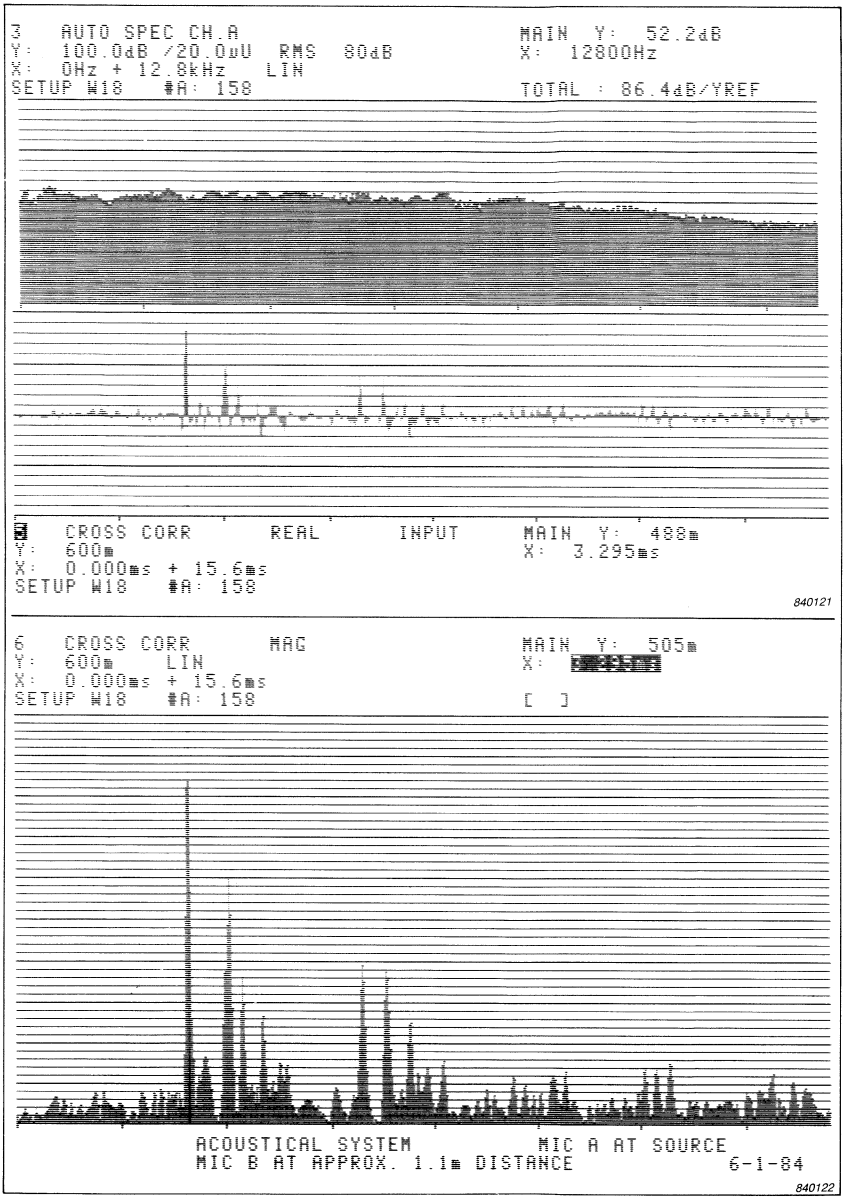

Fig. 44. The input Autospectrum of a broadband random noise signal from a sound source (upper graph). Real valued $\rho_{ab}(\tau)$ (middle graph). Magnitude of the complex $\vec{\rho}_{ab}(\tau)$ (lower graph)

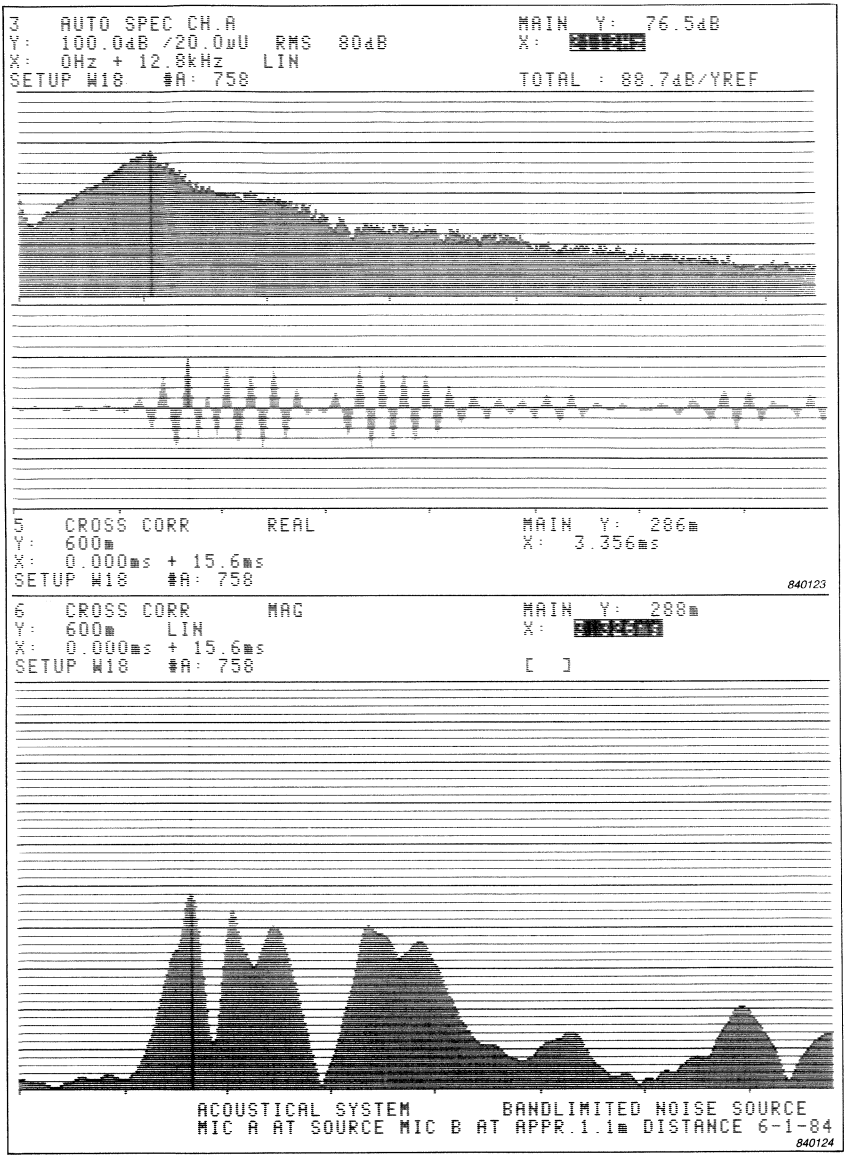

Fig. 45. The input Autospectrum of a band limited random noise signal from the sound source (upper graph). Real valued $\rho_{ab}(\tau)$ (middle graph). Magnitude of the complex $\overset{\vee}{\rho}_{ab}(\tau)$ (lower graph)

n other words, the signals have to be so broadband that the peaks in he Cross Correlation Function become narrow and separated, exactly as discussed for application of Autocorrelation Function for detection of echoes.

For the same reasons, as those mentioned for the analytical Impulse Response Function $\overset{\nabla}{h}(t)$ in Section 6, it is an advantage in many situations to work with the analytical Autocorrelation Coefficient Function $\overset{\nabla}{\rho}_{aa}(\tau)$ and the analytical Cross Correlation Coefficient Function $\overset{\nabla}{\rho}_{ab}(\tau)$ rather than with the real valued $\rho_{aa}(\tau)$ and $\rho_{ab}(\tau)$. These are defined by:

$$\overset{\nabla}{\rho}_{aa}(\tau) = \rho_{aa}(\tau) + j\tilde{\rho}_{aa}(\tau) \tag{7.8}$$

and

$$\overset{\nabla}{\rho}_{ab}(\tau) = \rho_{ab}(\tau) + j\tilde{\rho}_{ab}(\tau) \tag{7.9}$$

where $\tilde{\rho}_{aa}(\tau)$ and $\tilde{\rho}_{ab}(\tau)$ are the Hilbert Transforms of $\rho_{aa}(\tau)$ and $\rho_{ab}(\tau)$ respectively. The lower graphs in Fig.44 and 45 show the magnitude of the analytical Cross Correlation Coefficient Functions corresponding to the real valued Cross Correlation Coefficient Functions

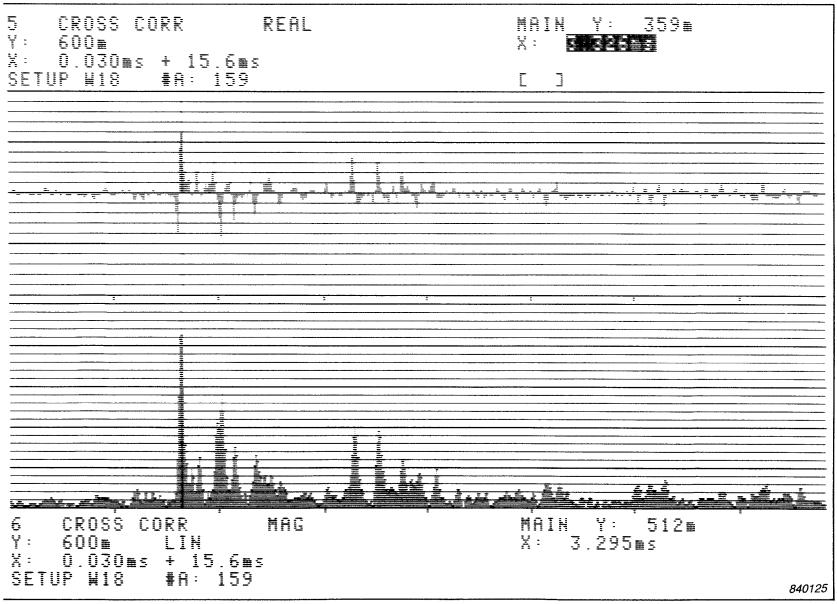

Fig. 46. Same results as for Fig.44, but obtained with zoom analysis between 512 and 13312 Hz

shown in the graphs in the middle. The peaks are easier to identify since the oscillations in $\rho_{ab}(\tau)$ are avoided. This is specially an advantage in the situation with band limitation as in Fig.45. If a zoom analysis is performed, the magnitude $|\hat{\rho}_{ab}(\tau)|$ should also be used for measurement of the peak amplitudes for the different reflections, since the real part $\rho_{ab}(\tau)$ might not peak where $|\hat{\rho}_{ab}(\tau)|$ peaks. Fig.46 illustrated this where the exact same signals as in Fig.44 are analysed, however using a zoom analysis from 512 Hz to 13312 Hz. This frequency range covers all the important information as does the baseband frequency range used in Fig.44. In the real part $\rho_{ab}(\tau)$, an amplitude for the peak at 3,3 ms is found to be 0,36, while the magnitude $|\hat{\rho}_{ab}(\tau)|$ gives an amplitude of 0,51 which is the same as the amplitude found in Fig.44.

In Fig.47 the magnitude of the Cross Spectrum $G_{AB}(f)$ and the magnitude of the Cross Correlation Coefficient Function are shown for the same signals, as those analyzed by use of the Impulse Response Function in Fig.37 (Section 6). The main reflections can still be seen in the Cross Correlation Coefficient Function, but their peaks are so

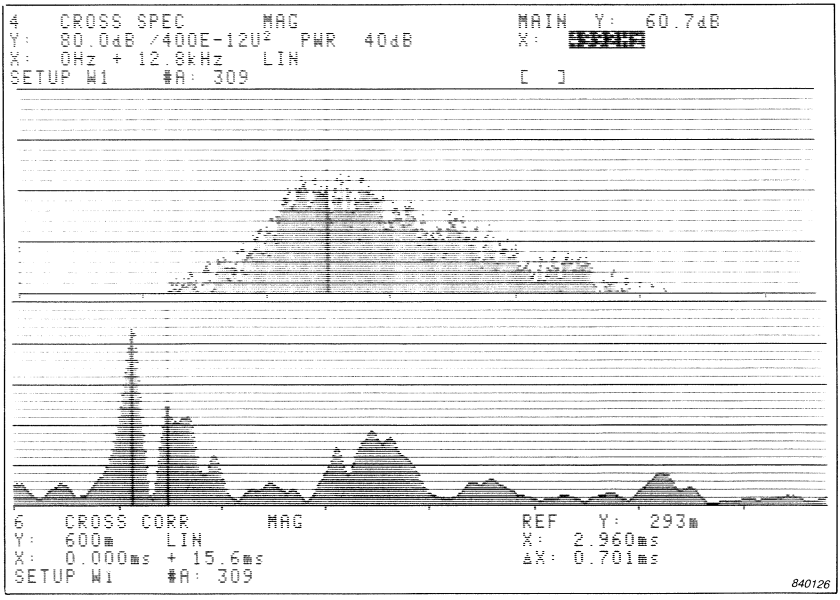

Fig. 47. Magnitude of Cross Spectrum and Magnitude of Cross Correlation Coefficient Function of the same signals as those analyzed by Impulse Response Function in Fig.37.

meared out, due to the band limitation seen in the Cross Spectrum, that ome of the smaller reflections are not detected. Fig.37 shows that the npulse Response Function is insensitive to this band limitation of the nput signal, since it describes the system independent of the signals nvolved.

lote that there has to be some power in the input signal at all the requencies in the analysis bandwidth, before a well-defined Frequency esponse Function (and thereby a well-defined Impulse Response Function) can be computed.

Since we are working with the DFT (or rather FFT) which computes the pectra at discrete frequencies, the effect of circular correlation has to e taken into account. As a consequence of computing the spectra at liscrete frequencies $k\Delta f = k\,1/T$, the time signals are artificial period ignals ranging from $-\infty$ to $+\infty$ with the time record in the analyzer of ength T being the period length. The computed Correlation Functions re the Correlation Functions of these artificial periodic time signals lisplaced relative to each other, and a circular correlation effect, as hown in Fig.48, will appear. The end of one signal (end of the period in ne signal) will overlap with the beginning of the other signal (the eginning of the period in the other signal) and the estimated Correlation unction will be incorrect. In Fig.48 (lower graph) the Correlation Func-

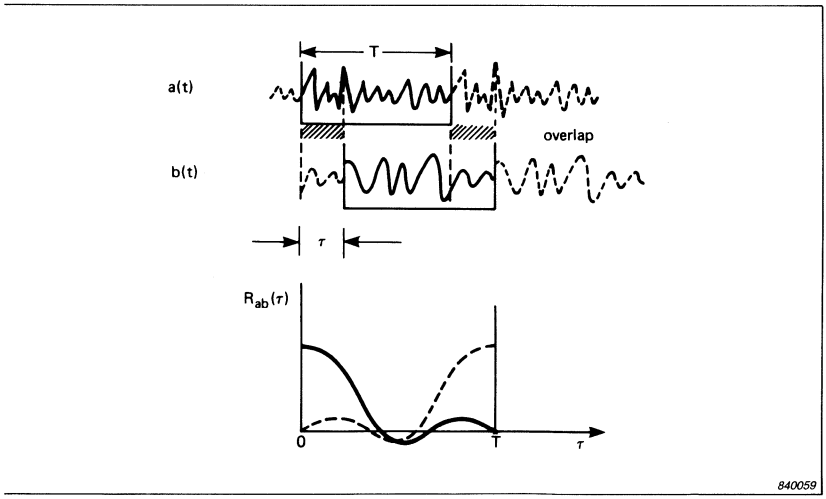

ig. 48. Circular correlation effect. The Correlation Function is assumed to be even in the lower graph

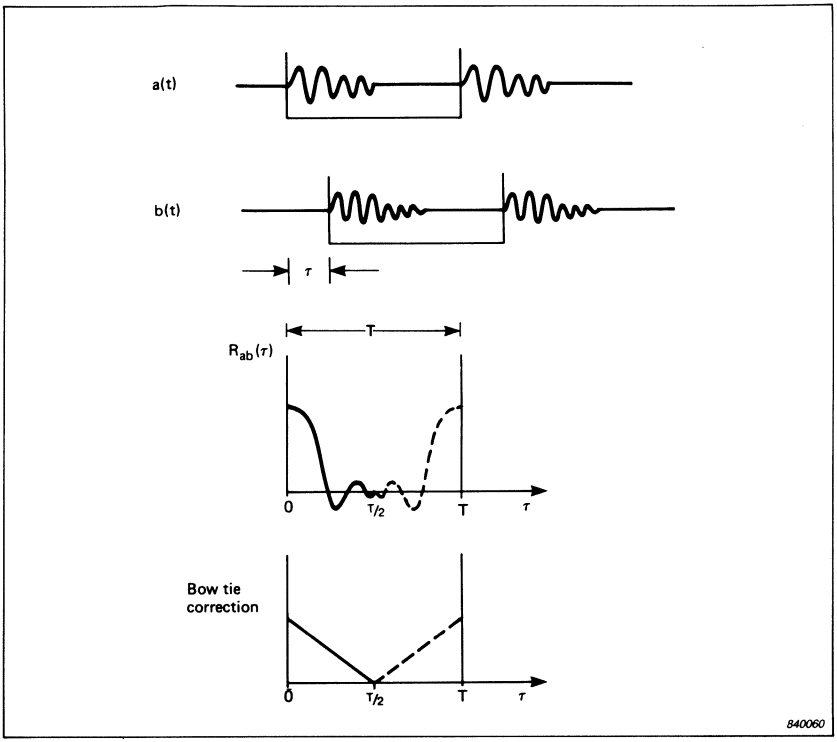

Fig. 49. Zero pad of the time records in order to avoid the effect of the circular correlation shown in Fig.48. The bow tie correlation is shown in the lower graph

tion between the two signals is assumed to be even, which is not the case in general for Cross Corrleation Functions. This problem of circular correlation is overcome by setting the signal equal to zero in the second half of the record as illustrated in Fig.49. This is called "zero pad". The zero pad will, however, also cause the estimated Correlation Function to be biased, but the bias error is known and can be corrected for. Due to the artificial nullifying of the signals in the last half of the record the estimated Correlation Function $\hat{R}(\tau)$ will be lower than the true Correlation Function $R(\tau)$, the extent depends upon the displacement τ. The relation is

$$\hat{R}(\tau) = \frac{|\, T/2 - \tau \,|}{T/2} R(\tau) \quad ; \quad 0 \leqslant \tau \leqslant T/2 \tag{7.10}$$

assuming rectangular weighting in the analysis.

Correction for the factor $\frac{|T/2 - \tau|}{T/2}$ is called the "bow tie" correction (see Fig.49) and can be applied as a post-processing after the measurement.

In Fig.49 the Correlation Function $R(\tau)$ is assumed to be even (as in Fig.48), which only in general is true for Autocorrelation Functions.

In all the measurements shown in this Section, zero pad and rectangular weighting has been used.

If the signals involved are transients with a duration shorter than $T/2$, the bow tie correction should obviously not be used.

3. Sound Intensity

The sound intensity is a vector quantity $\vec{I}$ describing the direction and the amount of the net flow of acoustic energy at a given position in a sound field.

A dual channel FFT measurement of the sound pressure signals from two closely spaced microphones can be used for calculation of the sound intensity. The calculated intensity is the component I_r of the intensity vector $\vec{I}$ in the direction given by the line joining the acoustic centres of the two microphones.

Fig.50 shows a microphone probe where the two microphones are placed in a face to face configuration (the B&K Sound Intensity Probe Type 3519). This sound intensity probe features very little disturbance of the sound field. The shadowing effect of one microphone on the other is minimal and the effective separation between the microphones is well

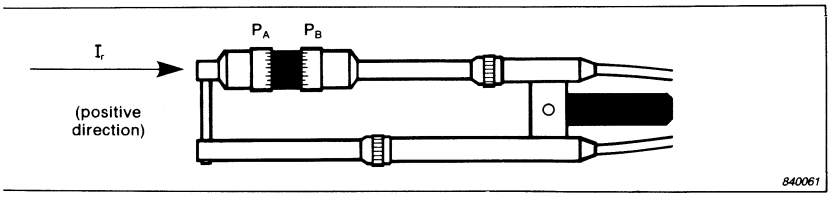

Fig. 50. Two microphone sound intensity probe (B&K Type 3519) with the microphones in face to face configuration. The component I_r of the sound intensity vector $\vec{I}$, is measured positive in the direction indicated by the arrow (from microphone A to microphone B)

defined. A side by side configuration of the microphone is also used sometimes, for instance in situations where the space is very confined or when measurements has to be performed as close as possible to a surface.

It can be shown that the intensity component I_r, with the direction from microphone *A* to microphone *B* defined as the positive direction, is given by

$$I_r = -\frac{1}{\omega \rho \Delta r} \; Im \left\{ G_{AB}(f) \right\} \tag{8.1}$$

where $Im \left\{ G_{AB}(f) \right\}$ is the imaginary part of the one-sided Cross Spectrum between the two sound pressure signals $p_A(t)$ and $p_B(t)$, ρ is the density of air and Δr is the spacing between the microphones. The air density is given by the ambient pressure p (in mbar) and the air temperature t (in °C) via the formula

$$\rho = 0{,}3485 \; \frac{p}{273 + t} \quad \left[\frac{kg}{m^3} \right]$$

In the B&K Analyzers Types 2032 and 2034, the microphone spacing Δr, the ambient pressure p and temperature t are entered from the front panel and the sound intensity is calculated according to (8.1) from the basic dual channel measurement. The sound pressure Autospectra $G_{AA}(f)$ and $G_{BB}(f)$ are therefore available as well from the same measurement. The reactivity of the sound field defined as $L_K = L_I - L_P$, where L_I is the intensity level (in dB relative to $1\,pW/m^2$) and L_p is the sound pressure level (in dB relative to $20\,\mu$Pa), can be checked from the same measurement. The reactivity L_K should always be checked, since it is one of the factors which determines the statistical errors in the intensity estimates and should be within the dynamic range of the analysis. For a plane wave propagating in free field the reactivity is zero dB ($L_P = L_I$) and the sound field is called an active sound field. In an ideal diffuse field the intensity is zero and the sound field is purely reactive.

The sound intensity can also be calculated directly in real time using the formula

$$I_r = -\frac{1}{2 \rho \Delta r} \; \overline{\left(p_A + p_B \right) \int \left(p_B - p_A \right) dt} \tag{8.2}$$

where the bar indicates time averaging and p_A and p_B are the sound pressure time signals as before. This approach is implemented using 1/3 octave and 1/1 octave (and 1/12 octave) digital filters in the B&K Intensity Analyzer Type 3360.

Compared to this technique one of the advantages of using the two channel FFT approach to sound intensity is that, since the spectrum is calculated in narrow bands with constant bandwidth, this method is very suitable for detection and recognition of pure tones, in a sound field. There might be several closely spaced pure tones, coming from different directions, which can only be separated using narrow band analysis, assuming that these frequency components are sufficiently stable. Harmonic related frequency components in the sound field can also easily be identified using constant narrow bandwidth and a linear frequency scale. Fig.51 shows an example where the B&K Analyzer Type 2032 is used. The sound intensity is shown on a socalled bipolar display, where positive intensity components point upwards in the upper half of the display and negative intensity components point downwards in the lower half of the display. One sound source is seen to radiate harmonic related frequency components in a direction towards the front of the probe and gives a resulting positive intensity level at these frequencies. Another source, which radiates broadband random noise in the opposite direction at the probe position, is causing the net flow of acoustical energy, in the direction of the probe, to be negative at the other frequencies.

One of the disadvantages of using the two channel FFT approach as opposed to the digital filter method is that the analysis can only be performed in real time in a limited frequency span. Since Hanning weighting is used when analyzing normal continuous signals, there has

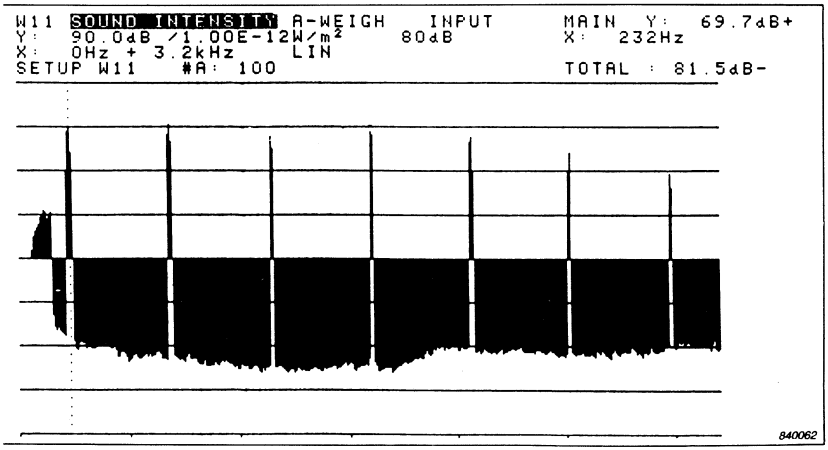

Fig. 51. Example of a narrow band sound intensity spectrum, calculated from a two channel measurement (B&K Analyzer Type 2032 or 2034)

to be 75% overlap of the time records in order to get true real time analysis, i.e. a resulting (overall) weighting function on the time signals which is flat (see Ref.16). This means for instance that for the high speed B&K Analyzer Type 2032 a true real time analysis can only be performed in a frequency span which is not wider than $\sim 1/4 \times 5$ kHz. The digital filter Analyzer Type 3360 will always work in real time up to 10 kHz in the 1/3 octave and 1/1 octave mode.

Another disadvantage of the two channel FFT approach is that longer averaging time is needed in order to get the same statistical accuracy in the measurement as by use of the digital filter analyzer, except for very low frequencies. The broader bandwidths of the 1/3 octave or 1/1 octave filters give an averaging in frequency which will decrease the random error (see Section 9). Specially if the sound field is very reactive (high sound pressure level compared to the intensity level) as in diffuse sound fields, the sound intensity measurement using two channel FFT can be very time consuming in order to obtain a certain statistical accuracy of the estimated sound intensity spectrum.

Consider an example where a number of averages n_d = 500 is required in order to get a specified statistical accuracy.

a) FFT Method:
   Let us assume that we are working with a frequency span which is so wide that the analysis time for computing one sound intensity spectrum, is longer than the record length in the analyzer. For the high speed B&K Analyzer Type 2032, this means that the frequency span is wider than 5 kHz. One sound intensity spectrum is computed approximately every 160 msec giving a total analysis time of $T_{total} \approx 500 \times 160$ msec = **1 min 20 sec.**

b) Digital Filter Method:
   $n_d = 500$ is equivalent to a BT product (Bandwidth × Averaging Time) of 500. For the 1/3 octave at 1 kHz, for instance, B ≈ 230 Hz and the total analysis time is therefore $T_{Total} = \frac{500}{B} \approx$ **2,2 sec**. For the 1/3 octave filter at 10 kHz, $T_{Total} \approx$ **0,22 sec** and for the 1/3 octave filter at 100 Hz, $T_{Total} \approx$ **22 sec.**

For many applications it is also much easier to handle and interpret the reduced amount of data from a 1/3 octave or a 1/1 octave analysis. Since acoustic measurements are often specified in 1/3 octave or 1/1 octaves, an analysis using the system with the standardized filters would be preferred.

Finally it should be mentioned that the digital filter system Type 3360 is a dedicated intensity measurement system giving some practical advantages for the user, such as a remote control unit and a separate display unit.

The basic limitations in the two microphone approach to analysis of sound intensity are the same for both systems. The finite distance Δr between the two microphones gives an upper bound for the useful frequency range in the analysis, and the phase mismatch between the two channels in the measurement system, including the microphones, gives a lower limit on the frequency range. A discussion of this is found in Ref.15 and 22.

The principal applications of sound intensity are: a) sound power determination, b) ranking of noise sources, c) noise source location (for this purpose it is often useful to make an intensity mapping in terms of contour plots or 3–D plots, made by use of further post-processing and plotting routines), d) transmission loss determination, e) sound absorption measurements.

Examples of these applications are dealt with in the References [15, 20, 21, 27–30] and will not be discussed further in this article.

9. Statistical errors in the estimates

When the analysis is performed on random signals (time histories) the different functions derived from a dual channel FFT measurement are estimated with limited accuracy. It is here assumed that we have stationary, continuous or transient random signals, which are band-limited Gaussian distributed white noise signals over the analysis bandwidth.

Averaging of the Autospectra and the Cross Spectrum is performed over only a finite number of records n_d giving the estimates $\hat{S}_{AA}(f)$, $\hat{S}_{BB}(f)$ and $\hat{S}_{AB}(f)$ of $S_{AA}(f)$, $S_{BB}(f)$ and $S_{AB}(f)$ by:

$$\hat{S}_{AA}(f) = \frac{1}{n_d} \sum_{i=1}^{n_d} \hat{A}_i^{\star}(f) \cdot \hat{A}_i(f) \tag{9.1}$$

$$\hat{S}_{BB}(f) = \frac{1}{n_d} \sum_{i=1}^{n_d} \hat{B}_i^{\star}(f) \cdot \hat{B}_i(f) \tag{9.2}$$

$$\hat{S}_{AB}(f) = \frac{1}{n_d} \sum_{i=1}^{n_d} \hat{A}_i^*(f) \cdot \hat{B}_i(f) \tag{9.3}$$

From these two-sided spectral density estimates, the one-sided spectral density estimates $\hat{G}_{AA}(f)$, $\hat{G}_{BB}(f)$ and $\hat{G}_{AB}(f)$ are calculated according to (2.8) and (2.9) (Part I of the article, Section 2).

The errors can be divided into two types, bias errors $b[\hat{X}]$ and random errors $\sigma[\hat{X}]$, where $\hat{X}$ is the estimate of the true value X. A bias error $b[\hat{X}]$ is a systematic error introduced either in the measurement or in the analysis (post-processing). In some situations a bias error can be estimated either by performing certain measurements (of phase and gain differences in the two instrumentation channels for instance) or from theoretical calculations. The bias error can in such situations be corrected for, but this is not the case in general.

The random error $\sigma[\hat{X}]$ is the standard deviation of the estimates $\hat{X}$ and is due to the fact that averaging is not performed over an infinite number of records i.e. over infinitely long time, as shown in (2.4), (2.5) and (2.7). Averaging over the finite number of records n_d causes a random scatter in the estimates.

The bias error $b[\hat{X}]$ is defined by:

$$b[\hat{X}] = E[\hat{X}] - X \tag{9.4}$$

while the random error is defined as the standard deviation of $\hat{X}$ and therefore given by (see (3.3) in Section 3):

$$\sigma[\hat{X}] = \sqrt{E\left[\left(\hat{X} - E[\hat{X}]\right)^2\right]} \tag{9.5}$$

$E[\quad]$ means "expected value of" and X is the true value.

Often it is more practical to work with the normalized errors instead of the absolute errors $b[\hat{X}]$ and $\sigma[\hat{X}]$. The normalized bias error ϵ_b and the normalized random (standard) error ϵ_r gives the error as a fractional portion of the true value and are defined by:

$$\epsilon_b = \frac{b[\hat{X}]}{X} \tag{9.6}$$

$$\epsilon_r = \frac{\sigma[\hat{X}]}{X} \tag{9.7}$$

It is assumed that $X \neq 0$.

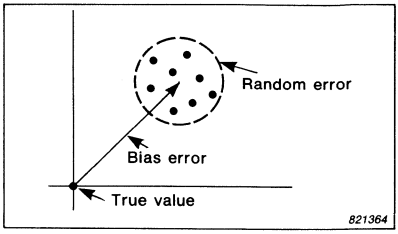

Fig. 52. Illustration of bias error and random error

Fig.52 gives an illustration of how a bias error and a random error influences the estimates of a value.

Bias errors in the different functions can be due to several effects such as

a) Extraneous noise at input and/or at output.
b) Other inputs to system which are correlated with measured input.
c) Leakage (resolution bias).
d) Non-linearities.
e) Propagation time delays not compensated for.

The effects of a), b) and c) were dealt with for the Frequency Response Function estimates in Section 4 and the influence of non-linearities were mentioned in Sections 3 and 5, and shall therefore not be discussed further here. If there is a propagation time delay τ from input to output of the system, this time delay has to be set between the records in the dual channel FFT measurement (see Fig.13 Section 3). Otherwise the Cross Spectrum will be biased with a factor of $(1 - \tau/T)$, where T is the record length in the analysis. Thus

$$\hat{G}_{AB}(f) \approx (1 - \tau/T)\, G_{AB}(f) \quad , \quad 0 \leq \tau \leq T \tag{9.8}$$

The functions derived from the Cross Spectrum will therefore also have a bias error,for example, the Coherence Function estimate is given by

$$\hat{\gamma}^2(f) \approx (1 - \tau/T)^2\, \gamma^2(f) \quad , \quad 0 \leq \tau \leq T \tag{9.9}$$

The random errors will now be discussed for the Autospectral and Cross Spectral density estimates and for the estimates of Coherence Function and Frequency Response Functions. These formulae were developed by Bendat and Piersol (Ref. [23] and [24]). The random errors associated with the sound intensity measurements will also be given.

The distribution of the data is assumed to be Gaussian (normal). This is a fair assumption when the random error ϵ_r is small. The filtering (FFT analysis) also tends to make the distribution of the time data closer to the Gaussian distribution.

For Gaussian distributed estimates $\hat{X}$ (without any bias error ϵ_b) it can be shown that there is approximately 68% chance of the true value X to be within the interval,

$$\hat{X}(1-\epsilon_r) \leq X \leq \hat{X}(1+\epsilon_r) \tag{9.10}$$

and approximately 95% chance of the true value to be within the interval

$$\hat{X}(1-2\epsilon_r) \leq X \leq \hat{X}(1+2\epsilon_r) \tag{9.11}$$

9.1. Auto Spectral and Cross Spectral density estimates

If averaging is performed over n_d time records of the random signals $a(t)$ and $b(t)$, the normalized random (standard) error for a frequency component of the Autospectral density estimates $\hat{G}_{AA}(f)$ and $\hat{G}_{BB}(f)$ at any frequency is given by

$$\epsilon_r\left[\hat{G}_{AA}(f)\right] = \epsilon_r\left[\hat{G}_{BB}(f)\right] = \frac{1}{\sqrt{n_d}} \tag{9.12}$$

Notice that the random error is independent of frequency. n_d corresponds to the socalled BT-product (product of analysis bandwidth B and total effective time record length T_{Total}) for the analysis. If rectangular weighting is used in the analysis we have $B = \Delta f = 1/T$ and $T_{\text{Total}} = n_d\, T$, giving $B \cdot T_{\text{Total}} = \frac{1}{T}\, n_d\, T = n_d$. T is the record length for each analysis.

If a smooth weighting function such as the Hanning weighting is used, the bandwidth B will be wider than Δf. The effective time length T_{eff} of each record will, however, be correspondingly shorter than T, due to the time weighting function. For each independent record, $B \cdot T_{eff}$ will be unity and therefore $B \cdot T_{total} = B \cdot T_{eff} \cdot n_d = n_d$.

Since the effective time length is shorter than T when Hanning weighting is used, averaging of spectra estimates from time records having some overlap (50% or 75% overlap for instance) will allow for a higher BT-product i.e. a higher number n_d, compared to an analysis performed with rectangular weighting for a given amount of time data, see Ref. [16].

The magnitude $|G_{AB}(f)|$ of the Cross Spectral density $G_{AB}(f)$ will at any frequency be estimated with a normalized random error of

$$\epsilon_r\left[\,|\hat{G}_{AB}(f)|\,\right] = \frac{1}{\sqrt{\gamma^2(f)\,n_d}} \tag{9.13}$$

where $\gamma^2(f)$ is the Coherence Function.

The lower the Coherence is in the measurement the more averaging is required in order to obtain a certain statistical accuracy in the estimate.

This is intuitively clear due to the fact that the lower the Coherence is the more random variation will there be in the individual estimates $\hat{A}_i^*(f) \cdot \hat{B}_i(f)$ (see Fig.4 and 9, Section 2 and 3).

9.2. Coherence Function estimates

The Coherence Function $\gamma^2(f)$ will also be estimated with only a limited accuracy from the Autospectral and Cross Spectral density estimates.

$$\hat{\gamma}^2(f) = \frac{|\hat{G}_{AB}(f)|^2}{\hat{G}_{AA}(f)\quad\hat{G}_{BB}(f)} \tag{9.14}$$

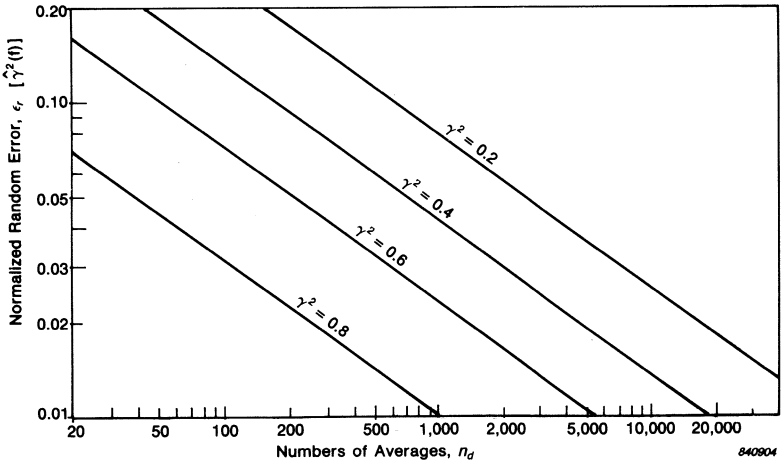

Fig. 53. Normalized random error $\epsilon_r[\,\hat{\gamma}^2(f)\,]$ of Coherence Function estimates as a function of number of averages n_d, for different values of (true) Coherence $\gamma^2(f)$

The normalized random (standard) error is given by

$$\epsilon_r \left[\hat{\gamma}^2(f) \right] = \frac{\sqrt{2}\left(1-\gamma^2(f)\right)}{\sqrt{\gamma^2(f)\, n_d}} \tag{9.15}$$

If the number of averages $n_d = 1$, we have that

$$\hat{\gamma}^2(f) = \frac{|\hat{A}_i^*(f)\ \hat{B}_i(f)|^2}{|\hat{A}_i(f)|^2\ |\hat{B}_i(f)|^2} = \frac{\hat{A}_i^*(f)\ \hat{A}_i(f)\ \hat{B}_i^*(f)\ \hat{B}_i(f)}{\hat{A}_i^*(f)\ \hat{A}_i(f)\ \hat{B}_i^*(f)\ \hat{B}_i(f)} = 1$$

Some averaging will therefore always have to be performed in order to estimate the Coherence Function. Even if the Coherence is unity, averaging is required to verify this in a measurement.

Fig.53 shows the relationship between the normalized random error $\epsilon_r \left[\hat{\gamma}^2(f) \right]$ and the number of averages n_d for different values of (true) Coherence $\gamma^2(f)$.

9.3. Frequency Response Function Estimates

When the Frequency Response Function of an ideal system is estimated from $H_1(f)$ or $H_2(f)$ and the signals are random noise signals (bandwidth-limited, Gaussian distributed white noise signals) there is a random error in both magnitude and phase. The error depends upon the number of (independent) averages n_d and the Coherence $\gamma^2(f)$ in the measurement.

The normalized random error for the magnitude of the estimate $|\hat{H}(f)|$ ($|\hat{H}_1(f)|$ or $|\hat{H}_2(f)|$) is given by

$$\epsilon_r \left[|\hat{H}(f)| \right] = \sqrt{\frac{1-\gamma^2(f)}{\gamma^2(f)\, 2\, n_d}} \tag{9.16}$$

In Fig.54 the normalized random error $\epsilon_r \left[|\hat{H}(f)| \right]$ is plotted as a function of number of averages n_d for different values of Coherence $\gamma^2(f)$. The more uncorrelated noise there is in the measurement i.e. the lower the Coherence is, the more averages have to be performed in order to get a certain statistical accuracy.

Fig.55 shows the estimates of $|H_1(f)|$ and $\gamma^2(f)$ from a dual channel measurement on an electrical filter network with random noise excita-

on. 100 averages are performed. The estimated Coherence $\hat{\gamma}^2(f)$ at 76 Hz is 0,6, due to uncorrelated noise at the output. The random error f $\hat{\gamma}^2(f)$ is

$$\epsilon_r\left[\hat{\gamma}^2(f)\right] \cong \frac{\sqrt{2}\cdot 0{,}4}{\sqrt{0{,}6\cdot 100}} \approx 0{,}07.$$

he random error for $|\hat{H}_1(f)|$ at the same frequency is

$$\epsilon_r\left[|\hat{H}_1(f)|\right] \cong \sqrt{\frac{0{,}4}{0{,}6\cdot 200}} \approx 0{,}06$$

hich in dB is $\approx$ 0,5 dB.

hus there is 68% chance of the true value $|H_1(f)|$ at 176 Hz, to be ithin the interval (since we have no bias error, see Section 4.2)

$$,94\cdot|\hat{H}_1(f)| \leqslant |H_1(f)| \leqslant 1{,}06\,|\hat{H}_1(f)|$$

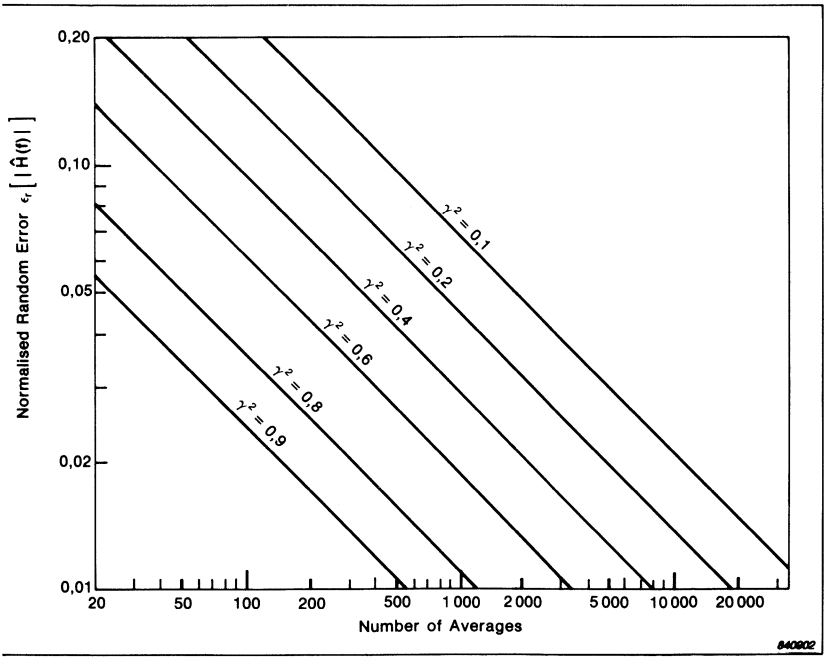

ig. 54. Normalized random error $\epsilon_r[|\hat{H}(f)|]$ of magnitude of Frequency Response Function estimates ($\hat{H}_1(f)$ or $\hat{H}_2(f)$) as a function of number of averages n_d for different values of Coherence $\gamma^2(f)$

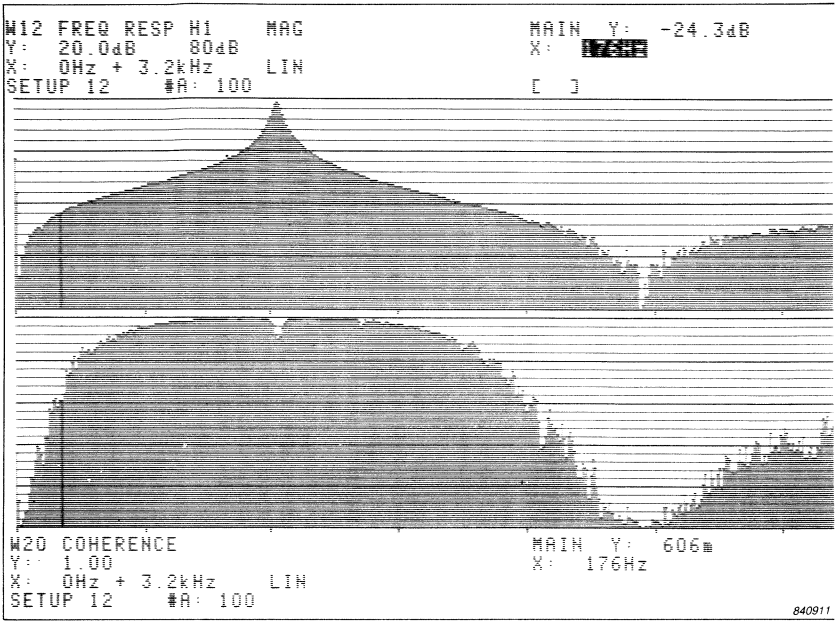

Fig. 55. Estimates of $|H_1(f)|$ and γ^2 from a dual channel measurement on an electrical filter network, with random noise excitation and 100 averages

or in dB

$$-24{,}8 \text{ dB} \leqslant |H_1(f)| \text{ (dB)} \leqslant -23{,}8 \text{ dB} \quad \text{since } |\hat{H}_1(f)| = -24{,}3 \text{ dB}.$$

The random errors at the same frequency for the Autospectra $\hat{G}_{AA}(f)$ and $\hat{G}_{BB}(f)$ and the magnitude of the Cross Spectrum $|\hat{G}_{AB}(f)|$, which are used for the calculations, are

$$\epsilon_r\left[|\hat{G}_{AA}(f)|\right] = \epsilon_r\left[|\hat{G}_{BB}(f)|\right] = \frac{1}{\sqrt{100}} = 0{,}10$$

and

$$\epsilon_r\left[|\hat{G}_{AB}(f)|\right] \simeq \frac{1}{\sqrt{0{,}6 \cdot 100}} \approx 0{,}13$$

Notice that these random errors are greater than the errors on the derived functions $\hat{\gamma}^2(f)$ and $|\hat{H}_1(f)|$.

The random error for the phase angle $\hat{\phi}(f)$ of $\hat{H}(f)$ can be approximated by

$$\sigma\left[\hat{\phi}(f)\right] \approx \epsilon_r\left[\,|\hat{H}(f)|\,\right] \tag{9.17}$$

hen the error $\epsilon_r\left[\,|\hat{H}(f)|\,\right]$ is small. $\phi(f)$ is measured in radians. The ue value $H(f)$ is here assumed, with 68% confidence, to be inside a ircle of radius $\sigma\left[\,|\hat{H}(f)|\,\right]$ and centered at $\hat{H}(f)$. Thus

$$\sigma\left[\hat{\phi}(f)\right] \approx \sin\left(\sigma\left[\hat{\phi}(f)\right]\right) \approx \frac{\sigma\left[\,|\hat{H}(f)|\,\right]}{|\hat{H}(f)|},$$

ving equation (9.17), for small $\sigma\left[\hat{\phi}(f)\right]$ or $\epsilon_r\left[\,|\hat{H}(f)|\,\right]$.

4 Sound Intensity

he sound intensity I_r (component in the direction of the probe) in a ındom sound field is as the other functions, estimated with a limited tatistical accuracy. The bias error basically depends on the spacing etween the microphones (high frequencies) and on the residual phase ıismatch between the two channels in the measurement system (low equencies). This is described in the references.

he random error is determined by the Coherence Function $\gamma^2(f)$ beveen the two sound pressure signals $p_A(t)$ and $p_B(t)$, the phase angle $_{AB}$ of the Cross Spectrum $G_{AB}(f)$ between the two signals and the umber of averages n_d. In Ref. [25] a formula for the normalized random rror $\epsilon_r\left[\hat{I}_r\right]$ is derived

$$\epsilon_r\left[\hat{I}_r\right] = \frac{1}{\sqrt{n_d}}\sqrt{\frac{1}{\gamma^2(f)} + \cot^2\left(\phi_{AB}(f)\right)\frac{1-\gamma^2(f)}{2\gamma^2(f)}} \tag{9.18}$$

alculations of Coherence $\gamma^2(f)$ and phase angle $\phi_{AB}(f)$ in different tuations are given in Ref. [26]. These calculations indicate that the ındom error $\epsilon_r\left[\hat{I}_r\right]$ mainly depends upon the reactivity L_K of the sound eld, defined as the difference between sound intensity level L_I and ound pressure level L_p, and also depends upon the interfering sound eld in the different situations (diffuse background noise or an interferg point source either perpendicular to or behind the probe, which oints towards the source of interest). The random error, however, was ound to be practically independent of the frequency and distance etween the microphones.

is therefore very important to check and report the reactivity of the ound field where the intensity measurements are performed, in order to e able to judge the validity of the results.

References

[12] THRANE, N. "The Hilbert Transform", B & K *Technica Review,* No.3 – 1984.

[13] BIERING H. & PEDERSEN, O. Z. "System Analysis and Time Delay Spectrometry", B&K *Technical Review*, No.1 and 2, 1983

[14] RANDALL, R. B. & HEE, J. "Cepstrum Analysis", B&K *Technica Review*, No.3, 1981.

[15] GADE, S. "Sound Intensity", B&K *Technical Review*, No.3 and 4, 1982.

[16] THRANE, N. "Zoom FFT", B&K *Technical Review* No.2, 1980.

[17] FAHY, F.J. "Measurement of Acoustic Intensity Using the Cross Spectral Density of two microphone signals.", Journal of the Acoustical Society of America 62(4 1057–1059, 1977.

[18] CHUNG, J.Y. "Fundamental Aspects of the Cross Spectrum method of measuring Acoustic Intensity". Senlis, 1981, pp.1–10.

[19] CHUNG, J.Y. & POPE, J. "Practical measurement of Acoustic Intensity – the two microphone cross spectral method" *Proc. Internoise* 1978 pp.893–900.

[20] GADE, S.,et al: "Sound Power determination using Sound Intensity measurements" (Part and II) B&K Appl. Notes.

[21] CROCKER, M.J. et al. "Application of Acoustic Intensity Measurements for the evaluation of Transmission loss of structures" Senlis 1981 pp.161–169.

[2] GINN, K.B. et.al. "Sound Power determination in highly reactive environments using sound intensity measurements", B&K Application Notes.

[3] BENDAT, J.S. & PIERSOL, A. G. "Random Data: Analysis and Measurement Procedures", Wiley–Interscience, 1971.

[4] BENDAT, J.S. & PIERSOL, A. G. "Engineering Applications of Correlation and Spectral Analysis", John Wiley & Sons, 1980.

[5] SEYBERT, A. F. "Statistical Errors in Acoustic Intensity Measurements", Journal of Sound and Vibration, 1981, 75, pp.519–526.

[6] DYRLUND, O. "A note on Statistical Errors in Acoustic Intensity Measurements.", Letters to the Editor, *Journal of Sound and Vibration*, 1983, 90, pp.585–589.

[7] NICOLAS, J., BENOIT, R., SAUVÉ, S. "Noise source identification and reduction in a chocolate plant", *Proceedings of Noise-Con.'83*.

[8] YANO, H., TACHIBANA, H., ISHII, K. "Application of sound intensity measuring technique to sound insulation measurements", *ICA* 1983.

[9] RASMUSSEN, G., RASMUSSEN,P. "Identification of energy sources and absorbers", *Proceedings of the 2nd International Modal Analysis Conference,* 1984.

[30] COLEMAN, R.B., HODGSON, T.H. "Acoustic Intensity Measurements on a 350 kN Automatic Punch Press", *Proceedings of Inter-Noise'83*.

News from the Factory

Dual Channel Signal Analyzers Type 2032/2034

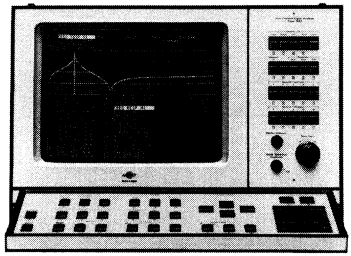

The Analyzers Type 2032 and Type 2034 combine the use of realtime, digital filtering techniques with a 2 k (2048 points) Fourier Analysis in two channels. Thus 801–line spectra are calculated with a chosen resolution from 1,95 mHz to 32 Hz selected in binary steps anywhere in the frequency range from DC to 25,6 kHz.

Both analyzers are extremely fast. The standard version, Type 2034, has a real-time bandwidth of 1,6 kHz in single channel mode and 800 Hz in dual channel mode. The high speed version, Type 2032, is approximately six times faster.

34 different functions are available such as Frequency Response, Impulse Response, Autospectra, Cross Spectrum, Correlation Functions, Enhanced Signals and their spectra, Distribution Functions, Coherence, Coherent Power, Sound Intensity, Cepstra, etc., etc. Most of these functions, including time domain functions, can be shown in 6 different formats: Real Part, Imaginary Part, Magnitude, Phase, Nyquist Plot and Nichols Plot. Two micro-processors are used in carrying out all the calculations: One for signal processing and the other for displaying (postprocessing) the data. Thus any function can be displayed at any time in any format and scaling, not only after a measurement has been completed, but also during a measurement.

The primary use of a dual channel analyzer is for system analysis, i.e. performing Frequency Response (and Impulse Response) measurements. Two different ways of calculating the Frequency Response Function are implemented in the 2032/2034: The traditional way $H_1 = G_{AB}/G_{AA}$ and the new way $H_2 = G_{BB}/G_{BA}$. H_1 suppresses uncorrelated noise at the output and gives the best estimate at anti-resonances. H_2 suppresses uncorrelated noise at the input and gives the best estimate at the resonance peaks.

The analyzers are equipped with extremely flexible trigger facilities.

A Free Running, Internal, External or manual trigger source can be selected in addition to a Generator trigger, where data collection is synchronized to the sequence of the built-in, zooming pseudo-random or impulse generator. Zooming random noise and a sine signal with a selectable frequency are also available.

Each channel can be independently set to have a Flat, Hanning, Transient, Exponential, Flat Top, Kaiser Bessel or User Defined weighting function. These weighting functions can even be applied to the Frequency Response Function, Cross Spectrum and Autospectra before calculating the Impulse Response, Cross Correlation and Autocorrelation functions.

The analyzers have seven cursor functions. Namely, Main Cursor, Harmonic Cursor, Sideband Cursor, Delta Cursor, Mask Cursor, Reference Cursor and even a Flex Cursor by which the x-axis can be scaled in any arbitrarily chosen engineering unit.

In spite of the high level of complexity and sophistication, the analyzers are very easy to use, because operation is largely self-explanatory with all relevant control settings clearly shown on its display screen, and because complete measurement and display setups can be stored for later recall and use.

The analyzers have a fully instrumented front end, by which they can accept signals from most B&K microphone preamplifiers, and via the Line Drive Amplifier Type 2644 from most accelerometers, force transducers and the Impact Hammer Type 8202 in either of its channels. In addition, the 2032/2034 are equipped with DC-coupled direct inputs for the input of electrical signals.

Output of the data which is displayed on a 12-inch large raster screen can be made to an X-Y recorder, a video recorder or to the B&K Graphics Recorder Type 2313, where a complete copy of the screen including graphs and alphanumerics are made in less than 10 seconds. The 2032/2034 are also equipped with an extremely flexible and sophisticated IEC 625–1/IEEE Std. 488–1978/ANSI MC 1.1–1975 interface which allows simple connection to most desk-top calculators.

Graphics Recorder Type 2313

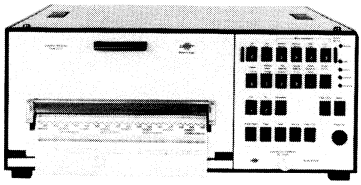

The Brüel & Kjær Graphics Recorder Type 2313 offers fast, fully annotated, graphic plots of measured frequency spectra and time functions as presented on the display screen of B&K Digital Frequency Analyzers, as well as documents measurement data transmitted by other equipment furnished with an IEC/IEEE interface.

For maximum operating flexibility, a range of interchangeable Application Packages is available. These plug-in the front of the 2313 and especially format data to suit different application requirements of B&K analyzing equipment. In addition, they permit a variety of special tasks to be carried for which extra equipment would normally be required. For example, several hundred complete measurement spectra can be stored in the Recorder for future print out or transmission to other equipment. Also, new types of measurement can be made using the 2313 to reformat stored and incoming data, plus use as a system controller is possible.

Where use as a conventional alphanumeric printer/graphics recorder is concerned, the 2313 may be operated without an Application Package. High-resolution graphic plots are made using a 512-point print head and as many as 128 (ISO 646 and 2022) characters may be printed. It accepts 50 m rolls of electrosensitive paper (metallized type) and from just one roll the equivalent of 160 A4 charts can be obtained.

PREVIOUSLY ISSUED NUMBERS OF BRÜEL & KJÆR TECHNICAL REVIEW

(Continued from cover page 2)

3-1977 Condenser Microphones used as Sound Sources.

2-1977 Automated Measurements of Reverberation Time using the Digital Frequency Analyzer Type 2131.
Measurement of Elastic Modulus and Loss Factor of PVC at High Frequencies.

1-1977 Digital Filters in Acoustic Analysis Systems.
An Objective Comparison of Analog and Digital Methods of Real Time Frequency Analysis.

4-1976 An Easy and Accurate Method of Sound Power Measurements.
Measurement of Sound Absorption of rooms using a Reference Sound Source.

3-1976 Registration of Voice Quality.
Acoustic Response Measurements and Standards for Motion-Picture Theatres.

2-1976 Free-Field Response of Sound Level Meters.
High Frequency Testing of Gramophone Cartridges using an Accelerometer.

1-1976 Do We Measure Damaging Noise Correctly?

4-1975 On the Measurement of Frequency Response Functions.

3-1975 On the Averaging Time of RMS Measurements (continuation).

SPECIAL TECHNICAL LITERATURE

As shown on the back cover page, Brüel & Kjær publish a variety of technical literature which can be obtained from your local B & K representative.

The following literature is presently available:

Mechanical Vibration and Shock Measurements (English), 2nd edition
Acoustic Noise Measurements (English), 3rd edition
Architectural Acoustics (English)
Strain Measurements (English, German)
Frequency Analysis (English)
Electroacoustic Measurements (English, German, French, Spanish)
Catalogs (several languages)
Product Data Sheets (English, German, French, Russian)

Furthermore, back copies of the Technical Review can be supplied as shown in the list above. Older issues may be obtained provided they are still in stock.

Printed in Denmark by Nærum Offset

BV 0014-11

Brüel & Kjær

DK-2850 NÆRUM, DENMARK · Telephone: + 45 2 80 05 00 · Telex: 37316 bruka dk